HEAT TRANSFER IN MULTI-LAYER ENERGETIC NANOFILM ON COMPOSITES SUBSTRATE

by

NAVID AMINI MANESH
B.S. Bahá'í Institute of Higher Education, 1996
B.S. University of Central Florida, 2005

A thesis submitted in partial fulfillment of the requirements
for the degree of Master of Science
in the Department of Mechanical, Materials and Aerospace Engineering
in the College of Engineering and Computer Science
at the University of Central Florida
Orlando, Florida

Summer Term
2007

ABSTRACT

The main purpose of this work is the physical understanding and the numerical description of the reaction of the dense metastable intermolecular composition (MIC). Energy density of MIC is much higher than conventional energetic material; therefore, MIC finds more applications in the propellant and explosive system. The physical model includes the speed of propagation and rate of reaction, and the relationship between the layer thickness, heat rate, and length of the flame based on physical model.

In Part I of this thesis, a one-dimensional model based on Weihs [1] was developed for 20 pairs of a multi-layer of aluminum and copper oxide. This problem was solved using an assumed value of constant atomic diffusion in Arrhenius' equation to obtain the velocity of self-propagation. Using the maximum and minimum measured velocities in a similar configuration, the activation energy was computed and was found to be significantly different. When the velocity was used to obtain a linear temperature profile, the margin of error was significant as well. Therefore, this method was seen to have severe shortcomings.

In Part II of this thesis, adiabatic unit cell of one layer of aluminum and copper oxide in an ideal reaction was considered. Temperature profile based on chemical heat generation and phase transformation of reactants has been calculated. This model confirmed the highest possible temperature during reaction of 2920 C ± 5% obtained in the literature, however, the model was unable to provide other important flame characteristics.

In Part III, a two-dimensional model was developed introducing the flame at the interface. A black box theory has been used to simplify some of the characteristics of the flame, ignoring

diffusion characteristics. Using this model, the length of flame was calculated using the measured value of the speed of propagation of the flame. Measuring some of the characteristics of the flame was the main goal of Part III of this thesis. Controllable environment was created for the multilayer thin film of aluminum and copper oxide to eliminate the number of effective variables that affect the speed of propagation. Transformable heat of reaction was used to control the speed of propagation. In addition, a MIC sample was designed and fabricated to measure the speed of propagation with an accuracy of 0.1 m/s. This measurement technique was used to measure the speed of propagation on variable substrate up to 65 m/s. The flame length was also calculated for different speeds of propagation over different substrates. The temperature distribution on the substrate was calculated numerically. Significant improvements have been made in Part III; however, this model does not provide concentration profiles.

For future work, a more complete two-dimensional physical model will be developed for self-propagation reaction of multilayer thin film of aluminum and copper oxide based on thermal transport and atomic diffusion. This two-dimensional model includes the reaction rate, speed of propagation and the temperature profile. Since this model relies on a number of physical variables that are as yet unknown, further work is warranted in this area to carry out a thorough computational study.

TABLE OF CONTENTS

LIST OF FIGURES

LIST OF TABLES

LIST OF NOMENCLATURE

α	Thermal Diffusivity
α_n	Harmonic Mean Thermal Diffusion Coefficient
ΔH	Energy Release of the Reaction
δ	Diffusion length ¼ of the Bi-Layer of Thin Film)
δ	Maximum Heat Penetration on Substrate
ρ	Density of the Mixture
λ	Thermal Diffusion Coefficient
ω	Length of Flame
A	Arrhenius Constant
C	Composition Profile
C_p	Specific Heat
D	Atomic Diffusion Coefficient
E	Activation Energy
h	Thickness of Silica on Composite Substrate
k	Thermal Conductivity
K_0	Bessel function of the second kind
k_n , α_n	Fourier Coefficients
k_e	Harmonic Mean Thermal Conductivity
M	Molecular Mass of Elements
m	Mass of Reactants
q	Heat Flux
R	Ideal Gas Constant
S_L	Regression Rate
T	Temperature
T_0	Initial Temperature
T_f	Final Temperature
v_x	Propagation Velocity of the Reaction in x Direction

CHAPTER 1
INTRODUCTION

Motivation

The high capacity of Metastable Intermolecular Composites (MIC) in propellants and explosives used by the US military are the main motivation of this study. Although traditional energetic compounds based on organic materials have similar energy per unit weight, MIC materials offer much higher energy density and capacity of the burn rate in comparison to the organic materials. This field of study is relatively young, yet it is showing a great promise and potential as an alternative substance for explosive and propellant systems. Energy density and burn rate are the two main mechanical criteria for evaluation and comparisons of energetic materials. Table 1.1 [2] shows energy per unit volume of traditional energetic materials in comparison to MIC.

Table 1-1 : Energetic Material Properties

Energetic Material	Energy per unit weight (kcal/gm)	Energy per unit volume (kcal/cm^3)[1]
TNT[i]	-1.09	-1.80
RDX[ii]	-1.51	-2.73
Al/CuO	-0.97	-4.98
Al/MoO_3	-1.12	-4.28

Although many earlier studies have shown the burn rate of MIC to be much lower than organic materials, a number of recent studies utilizing different technical processes and geometry

[i] 100% of theoretical maximum density is assumed.
[ii] Values are in terms of heat of detonation, which is the change in enthalpy for the high order detonation. No afterburning is considered.

of materials have improved the burn rate significantly [3-10]. These improvements have given hope and motivation to continue the intensity of the exploration in order to create a unified, consistent and predictable process. The challenge has been to theoretically explain the actual physical results of the experiments and improvements. It has been shown that a positive correlation exists between the geometry and deposition process of MIC and the burn rate. Theoretical analysis and modeling of the physical results show a good reason for utilization of MIC as an alternative energetic material for the explosive and propellant systems [10].

Upper limits for the burn rate of MIC materials have not been yet determined. There are a number of reports for the propagation speed of dense MIC materials and none shows rates higher than 20m/s [3,6,10]. In contrast, studies at the University of Central Florida have consistently achieved a burn rate as high as 65 m/s experimentally for multilayer thin film of aluminum and copper oxide. Higher burn rates may be achieved depending on the substrates used. Physical mechanisms can explain the speed of propagation and rate of reaction and help define some of the limitations and boundaries of the combustion process. It can also show better ways to process the samples in thin film scale.

Main Objective

The main objective of this study is to describe the physical processes of self-propagating reactions in multilayer thin films. A physical understanding of this process is the key point in defining some of the unknown variables influencing the reaction. Physical mechanism will be explained to understand the temperature distribution and speed of propagation and other effective variables. Mathematical models will be developed to quantify the results of physical experiments.

Standardized samples of MIC materials will be developed in order to measure and isolate the influencing variables of the experiment [11-22].

Problem Statement

A simplified reaction model of a multiple layer of Metastable Intermolecular Composite (MIC) of CuO and Al in on a standard substrate is proposed and will be solved in different stages. Three stages of solution are proposed in increasing complexity, and their strengths and shortcomings are discussed.

1) The specific objectives of the theoretical models and the experiment are as follows:

   In Chapter 2, the model of Weihs' [1] has been applied to 20 pairs of a multilayer of aluminum and copper oxide. This problem is solved using an assumed value of constant atomic diffusion in Arrhenius' equation to obtain the velocity of self propagation. Using the maximum and minimum measured velocities in a similar configuration, the activation energy is computed.

2) In Chapter 3, phase transformation (melting and vaporization) of the reactants during the reaction is considered. In this model, a single pair of aluminum and copper oxide layers in an ideal reaction is considered. An attempt is made to show step by step reaction in the adiabatic case of a standard layer of two materials. This study shows a number of phase transformations during the reaction, which compounds the difficulty of explaining the process through simple single-phase physical approach. While this model includes some complexity, it removes the earlier complexity of using multiple layers. Temperature profile based on chemical heat generation and phase transformation of reactants will be calculated. This model can confirm the highest possible temperature during reaction of

2920^{o}C ± 5% obtained in the literature. Various reference temperatures based on heat generation and phase transformation have been calculated for aluminum, copper, copper oxide and alumina. Modifying an existing model for the physical mechanism is the first attempt to explain the reaction.

3) The model developed in Chapter 3 is unable to provide important reaction characteristics such as burn rate, length of the flame and temperature profile. Therefore, in Chapter 4, a two-dimensional model is developed introducing the combustion phenomena and flame at the interface. A black box theory is used to simplify some of the characteristics of the flame, ignoring diffusion. In order to solve this conduction problem, speed of propagation is experimentally determined using a time-of-flight technique. Long strips of multilayer of aluminum and copper oxide in thickness of 26 nm and 54 nm, respectively, have been prepared by magnetron sputter deposition (Figure 1.1). Forty units of these strips forming a total thickness of 3.2 μm were used as the standard multilayer thin film. The substrate which is the main heat sink during the process has been changed based on the experimental process.

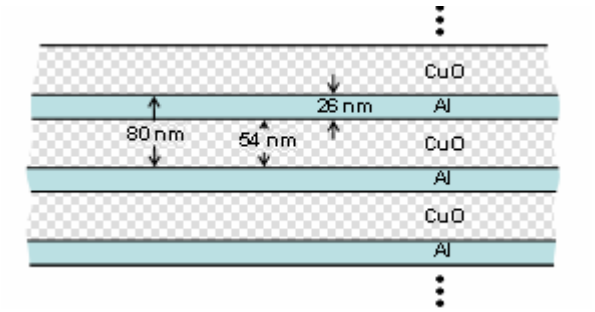

Figure 1-1 : CuO/Al MIC Layers

Estimating the length of flame, the maximum temperature and the penetration depth in single and composite substrates is calculated. Thus, a controlled environment is created for the

multilayer thin film of aluminum and copper oxide to eliminate the number of effective variables that affect the speed of propagation. The temperature distribution on the substrate is calculated numerically.

A number of variables can affect the MIC reaction process. To measure some of the characteristics and compare them, the number of variables should be reduced and isolated during the experiment. To control the heat front, a heat sink also called substrate is used. A number of materials with different thicknesses have been tested as a substrate for a standard thin film. Speed of flame front is measured in each case. The theory of moving heat source over the solid is used to model the process numerically. At this stage, linear heat sources are used as a simple flame front for a composite substrate. Linear heat sources move at the speed of the flame front. Heat that is generated at the interface on the thin film can be transferred to the substrate. A governing equation is developed to show the relationship between penetration depth and relative temperature. A numerical method is used to calculate the temperature profile based on the speed of propagation.

Literature Review

Combination reactions between chalcogen elements and metals are the most widely studied mechanically induced self-sustaining reactions. Takacs [23] summarized the result of a series of five papers by Chakurov and his collogues in 1980s, which represents the first results on self-sustaining reaction. Following these early studies, the field of mechanochemistry has had a rich history, which has led to the use of ball mills for processing a wide range of materials, ranging from minerals to advanced materials. Bakhshai et al. [24] used the ball milling method to demonstrate self- propagated reaction of mixture of Cu_2O and Al powders. Recently, the same group [25] developed the same type of reaction between Al and CuO.

Combustible multilayer materials are introduced by depositing alternating layers of materials, which react exothermically during thermally induced intermixing. Several research teams have studied analytical and theoretical processes of various layers and have introduced the general thermodynamic and kinetics of broad range of the thin film reactions.

The characterization of a self-propagating CuOx-Al in multilayer foil geometry was investigated. Armstrong's group [26-28] developed a model to find the heat rate of any possible multilayer reaction. This was later used by the Weihs' group. Based on the rate of reaction, a 1-D model can be used to calculate the heat transfer of reaction.

The experimental results showed that the highly exothermic nature of reaction is only a prerequisite for initiating combustion. Whether combustion takes place or not depends on the dynamic state of the reaction system. The influence of the crystalline structures of the reactants on the ignition of the combustion reactions instigated by high-energy ball milling is not always predictable. The calculation of the results of some reactions may be different due to internal and

external variables yet unknown. The factors influencing the outcome of the reaction and the variables are being studied. In this section, aluminum and copper oxide in a multilayer thin film and bulk reactions are discussed in detail as the selected, physical and numerical model; and also, a number of other investigations are highlighted and are discussed briefly.

Ball Milling

Mechano-chemical process (MCP) uses mechanical energy to activate chemical reaction and structural changes. Mechanically activated processes date back to the early history of humankind. The field of mechano-chemistry has had a rich history, particularly in Europe, which has led to the use of ball milling for processing a wide range of materials, ranging from minerals to advanced materials.

Self–propagating reaction was induced by ball milling in the mixture of Cu_2O and Al powder. Bakhshai et al. [24] presented the result of self–propagating reaction between Cu_2O and Al. Zeck et al. [25] continued the same type of reaction process with other materials. They investigated the self-propagating reaction between CuO and Al and compared the two results.

Bakhshai, et al. [29] used the ball milling method to demonstrate self-propagated reaction of mixture of Cu_2O and Al powders. Ball milling has been used to induce chemical reaction and alloying in variety of powder mixture. Three different reaction mechanisms have been observed.

1) In the case of the most exothermic condition, self-sustaining reaction is ignited in a few seconds after starting the ball milling process. Ignition does not require any external activation. The reaction self-propagates in the vial filled with large loose Al powder mass and large ball mass.

2) If the reaction cannot ignite or propagate in loose powder a self-sustaining reaction is ignited. After some activation time, the reaction starts in the powder layer covering the milling bodies, and its propagation depends on the balance between the reaction heat and heat transfer within the powder and from the powder to the environment.
3) Even if the reaction is exothermic enough to support a self-sustaining reaction, it may not happen if the amount of powder is too small. Consequently, the relatively large heat loss to the milling tools quenches any incipient reaction. In this case, a gradual mechano-chemical reaction is observed as a result of prolonged milling.

Zeck et al. [25] used the ball milling method to demonstrate self-propagated reaction of the mixture of CuO and Al powders. Self-propagating reaction of CuO and Al had been compared with Cu_2O and Al. All major components of their experiment were nearly similar.

Thin Film Reaction

Thin film reaction has increasingly played a main role in many of the new consumer electronic devices such as storage media, read and write heads, and flat panel displays. Such a remarkable array of applications has created a sense of excitement amongst the thin film scientists and engineers. Specifically, MIC materials are potentially better alternatives than organic materials for explosive and propellant systems. Michaelsent et al. [30] investigated the thermodynamics and kinetics of thin film reactions by using differential scanning calorimetry of several materials. The result of this research was published in 1997. Following that investigation Weihs' group [32-33] presented modeling and characterization of the propagation velocity of exothermic reaction in multilayer foils. They studied the CuO_x and Al reaction to identify the path and reaction kinetics. Experimental evidence showed that in the first reaction, CuO_x is

reduced to the mixture of CuO and Cu_2O which coalesces with an interfacial layer of Al_2O_3. They discovered two different paths of reaction in their studies and the results are as follows.

1) The exothermic reduction-oxidation reaction of CuO_x and Al to form Cu and Al_2O_3 were studied in multilayer foil. Using DTA, XRD, Auger depth profiling, and TEM, the reaction path and kinetics of the two-step reaction were analyzed [31].
2) Based on their experimental results, they were able to identify likely rate determining processes for each of the two reaction steps. In the first exothermic reaction, the lateral growth of Al_2O_3 nuclei appears to control the rate of heat generation and, therefore, the reaction rate. This reaction slows as nuclei impinge and end when a continuous layer has formed. The activation energy for this step of the reaction was calculated to be 2.9eV. Although CuO and Cu_2O are also reduced in this exothermic reaction, resulting in the formation of Cu layer, the heat generated is attributed to the formation of Al_2O_3 [31].
3) In the second stage of the CuO_x /Al reaction, diffusion of oxygen through the Al_2O_3 most likely controls the reaction rate in the first half of the exothermic reaction, and the heat generated is attributed to thickening of Al_2O_3 layers [32]. The rate of the reaction in the second half of the reaction, though, may also be limited by thickening of Cu product or non-uniform reduction in oxygen source, CuO_x.
4) Blobaum et al. [32] studied self-propagating formation reaction in multilayer foils and, they investigated one of the applications in joining and ignition. This work involves the multilayer foil reaction, which contains a reduction- oxidation thermite reaction between CuO_x and Al. We make the following observations and conclusions from their work.

- Thermite foils containing CuO_x and Al were sputter-deposited in a multilayer geometry [33]. The layered structure was confirmed using a variety of techniques including auger depth profiling and different TEM methods. The crystal structure of CuO_x is that of paramelaconite, Cu_4O_3, and XPS confirms that the oxide is indeed richer in copper than the CuO sputter target. Elemental maps show that oxygen is dispersed homogeneously in the CuO_x layer and, more importantly, that the concentration from oxygen in the Al layers is minimal because only a contribution from surface oxygen was detected. There is a narrow region at the interface between the two layers, which was identified as amorphous and nano crystalline Al_2O_3.
- DTA showed that the CuO_x/Al foils can react in highly exothermic manner, and there are two major exotherms, which appear during heating. The total heat released by the reaction is -3.9±0.9 kJ/g, which is similar to the heat of reaction calculated for the reaction of CuO and Al. Additionally, the heat released during the reaction is sufficient to permit the reaction to self- propagate along the foil at a velocity of 1 m/s. Products of the self- propagation reaction indicate that the reaction temperature of copper is 2846 K.
- The deposition of these thermite reactants in a distinct layered geometry opens the door for future research in reduction-oxidation mechanisms. Furthermore, the development of the processing method for CuO_x/Al foils and initial characterization of the reactions suggest that these materials can be used as local heat sources in a variety of joining applications.

Fischer and Grubelich [33] tabulated the experimental reference temperatures of the reaction of aluminum and copper oxide. Based on these data, he proposed the energy release of the reaction of aluminum and copper oxide to be 974.1cal/g.

Uncertainties in the Reaction of Aluminum and Copper Oxide

The influence of the crystalline structures of the CuO and Al on the ignition of the combustion and high-energy released in short amount of time is always accompanied by a certain amount of uncertainty amongst the path of reactions. Changing the path of reaction can change the product, which affects the amount of energy released in the chemical function. There are several studies show many other possibilities of reaction between CuO and Al. Three other possible paths for copper oxide and aluminum have been determined [34-36] and are given below.

1) The reduction reaction in the Al–10CuO mixed powders is induced by ball milling. CuO is believed to be reduced gradually by Al, controlled by diffusion of the atoms and ions. The reduced Cu metal reacts with Al spontaneously to form the metastable Al_4Cu_9 phase during ball milling, instead of the $CuAl_2$ phase, which is only observed after annealing.
2) A nanostructure Al–5CuO composite is obtained by hot pressing the mechanical alloy powders under conditions of relatively low temperature and high pressure. The reinforcements include $CuAl_2$ with size of 100–500 nm and oxide, carbide with sizes of 10–50 nm. The analysis reveals that the crystalline size of the Al matrix is 73.6 nm on average, which can be attributed to the retarding effects of the fine oxide on the grain growth of the Al matrix. Meanwhile, the fine oxide and carbide in the composite also promote the nucleation of $CuAl_2$, thus inhibiting the solution of Cu in Al.

3) The nanostructure Al–5CuO composite possesses high yield strength both at ambient and elevated temperatures. The fine grains of Al and the nano-sized oxide and carbide particles contribute mainly to the increased strength of the composite [36]. This paper investigated the type of crystal structure of product (FCC, BCC, HCP) can affect the total energy released in the reaction. There are many other examples of variations in the path and the results, and due to the nature of the variables, a certain amount of uncertainty is always expected [36].

Summary of Literature Search

In this section, a review of previous studies of aluminum and copper oxide in bulk and thin film geometry has been done. Most of the critical points of these studies are highlighted. Ball milling, one of the traditional activation techniques, was discussed for the bulk reaction of aluminum and copper oxide. There is evidence from the literature that thin films are a better and more effective option to increase the rate of reaction. In the last portion of this section, some of the unexpected chemical functions are briefly explained based on available information.

CHAPTER 2
ONE-DIMENSIONAL MODEL OF THE EXOTHERMIC REACTIONIN MULTILAYER FILMS

This chapter discusses the one-dimensional modeling and characterization of the propagation velocity of the exothermic reaction in multilayer foils. Mann et al. [32] developed a new model consisting of the so-called sandwich model of Armstrong and Koszykowski [26-28] by characterizing the rate of reaction for any multilayer pair of thin films. The sandwich model has a specific description for multilayer foils. Based on this description, the basic equation for atomic diffusion, and the general equation for thermal transport, they calculated the equation of the reaction rate of multilayer function.

The model, which was developed by [32], is the only classical approach for a multilayer geometry in thin film. Their experimental results for Al/Ni, support this numerical model. The physical model is explained below and two experimental values of the speed of propagation of the Al-CuO film were compared with the model. The corresponding temperature profiles for the two speeds are also compared.

Analysis

Description of multilayer foils

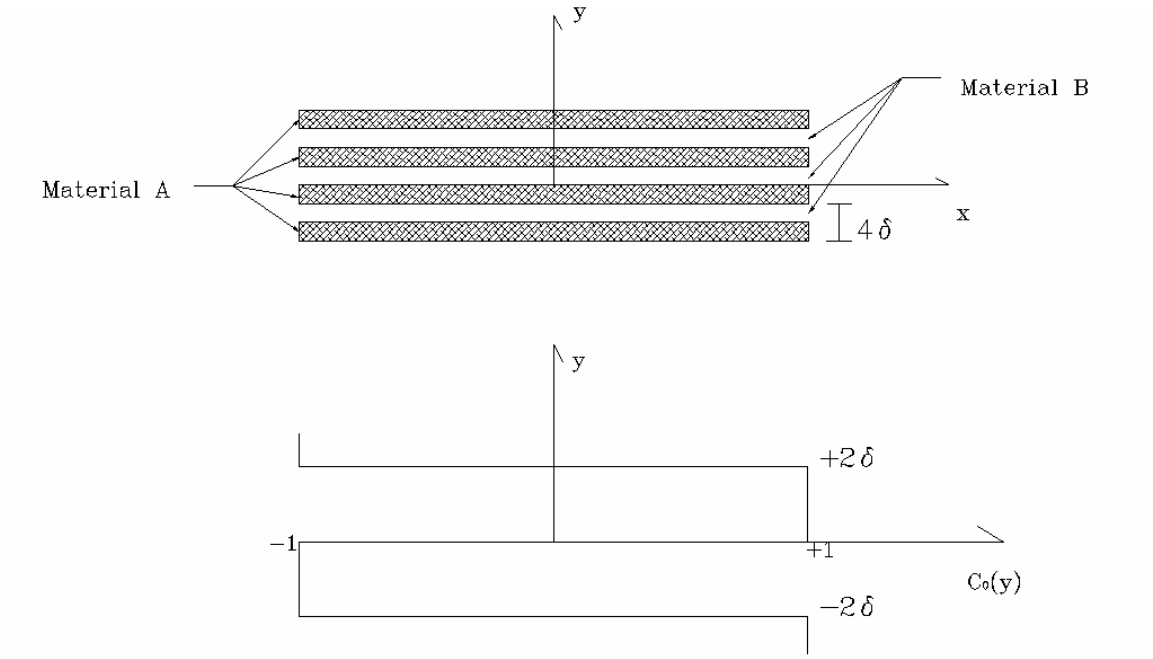

Figure 2-1 : Ideal profile for Composition, C

Material A: C=1

Material B: C=-1 (2.1)

Between layers: C=0

Theory of Atomic Diffusion

Basic Diffusion Function

$$\frac{dC}{dt} - \nabla D(\nabla C) = 0 \tag{2.2}$$

Sandwich Theory

C is function of x, y, z, t and propagation in x direction

$$\frac{dC}{dt} = \frac{\partial C}{\partial t} + V_X \frac{\partial C}{\partial x} \tag{2.3}$$

3-D Equation for composition, C:

$$\frac{dC}{dt} - \nabla D(\nabla C) = [\frac{\partial D(\frac{\partial C}{\partial x})}{\partial x} + D(\frac{\partial^2 C}{\partial x^2})] + [\frac{\partial D(\frac{\partial C}{\partial y})}{\partial y} + D(\frac{\partial^2 C}{\partial y^2})] + [\frac{\partial D(\frac{\partial C}{\partial z})}{\partial z} + D(\frac{\partial^2 C}{\partial z^2})] \tag{2.4}$$

Diffusion is neglected in y and z directions. Therefore,

$$\frac{\partial D(\frac{\partial C}{\partial y})}{\partial x} + D(\frac{\partial^2 C}{\partial x^2}) = 0 \tag{2.5}$$

$$\frac{\partial D(\frac{\partial C}{\partial z})}{\partial z} + D(\frac{\partial^2 C}{\partial z^2}) = 0 \tag{2.6}$$

$$\frac{\partial C}{\partial t} + V_X \frac{\partial C}{\partial x} + [\frac{\partial D(\frac{\partial C}{\partial x})}{\partial y} + D(\frac{\partial^2 C}{\partial y^2})] = 0 \tag{2.7}$$

Arrhenius Relationship

$$\frac{D}{\lambda} = A \cdot e^{\left(\frac{-E}{RT}\right)} \tag{2.8}$$

where,

λ = Thermal Diffusion Coefficient

D = Atomic Diffusion Coefficient

A = Arrhenius Constant

R = Ideal Gas Constant

E = Activation Energy

Substituting (2.8) in (2.7)

$$\frac{1}{\lambda}\frac{\partial C}{\partial t}+\frac{V_X}{\lambda}\frac{\partial C}{\partial x}+A.\frac{\partial\left(e^{\left(\frac{-E}{RT}\right)}\right)}{\partial y}\frac{\partial C}{\partial t}+A.e^{\left(\frac{-E}{RT}\right)}\frac{\partial^2 C}{\partial y^2}=0 \tag{2.9}$$

Steady state

$$\frac{1}{\lambda}\frac{\partial C}{\partial t}=0 \tag{2.10}$$

Temperature is constant along the y direction

$$\frac{\partial\left(e^{\left(\frac{-E}{RT}\right)}\right)}{\partial y}=0 \tag{2.11}$$

Substituting (2.10) and(2.11) in (2.9) (2.12)

$$\frac{V_X}{\lambda}\frac{\partial C}{\partial x}+A.e^{\left(\frac{-E}{RT}\right)}\frac{\partial^2 C}{\partial y^2}=0 \tag{2.13}$$

$$F=\int_{-\infty}^{x}e^{\left(\frac{-E}{RT}\right)} \tag{2.14}$$

Solving eq. (2.13) by separation of variables

$$C(F,y)=\sum_{n=odd}\left[k_n.\sin(\alpha_n y)e^{\left(-\alpha_n\lambda AF/v_x\right)}\right] \tag{2.15}$$

$k_n and \alpha_n$ are the Fourier coefficients and Eigen-values of the sine series for C_0(y) in Figure 1, and are given by:

$$\alpha_n = n\pi / 2\delta \tag{2.16}$$

$$k_n = 1/2\delta \int_{-2\delta}^{2\delta} C_0(y)\sin(\alpha_n y)dy \tag{2.17}$$

Thermal Transport

General thermal equation

$$c_p.\rho.\frac{dT}{dt} - c_p.\rho.\lambda.\nabla^2 T = \frac{dQ}{dt} \tag{2.18}$$

$$\frac{dT}{dt} = \frac{\partial T}{\partial t} + v_x \frac{\partial T}{\partial x} \tag{2.19}$$

For any chemical reaction

$$Q - Q_0 = c_P.\rho.(T_f - T_0) - \Delta C \tag{2.20}$$

Where ΔC is the heat released in reaching a composition C when starting from pure A and B (see fig.1)

$$\frac{d(Q - Q_0)}{dt} = \frac{d\left[c_P.\rho.(T_f - T_0)\right]}{dt} - \frac{d\Delta C}{dt} \tag{2.21}$$

$$\frac{d\left[c_P.\rho.(T_f - T_0)\right]}{dt} = 0 \tag{2.22}$$

$$\frac{dQ}{dt} = \frac{d\Delta C}{dt} \tag{2.23}$$

ΔC is only a function of x and time, based on the initial assumption

$$\frac{d\Delta C}{dt} = \frac{\partial \Delta C}{dt} + v_x \frac{\partial \Delta C}{\partial x} \tag{2.24}$$

Substituting (19) and (24) in (18)

$$c_p.\rho\left[\left(\frac{\partial T}{\partial x}+v_x\frac{\partial T}{\partial x}\right)-\lambda\nabla^2 T\right]=\frac{\partial \Delta C}{\partial t}+v_x\frac{\partial \Delta C}{\partial x} \tag{2.25}$$

T is function of x only. Therefore,

$$\nabla^2 T=\frac{\partial^2 T}{\partial x^2} \tag{2.26}$$

$$c_p.\rho\left[\left(\frac{\partial T}{\partial x}+v_x\frac{\partial T}{\partial x}\right)-\lambda\frac{\partial^2 T}{\partial x^2}\right]=\frac{\partial \Delta C}{\partial t}+v_x\frac{\partial \Delta C}{\partial x} \tag{2.27}$$

Assuming Steady state,

$$\frac{\partial \Delta C}{\partial t}=0 \tag{2.28}$$

Incorporating the approximation,

$$\frac{\partial T}{\partial x}\langle\langle\frac{\partial^2 T}{\partial x^2} \qquad\qquad v_x\frac{\partial T}{\partial x}\langle\langle\lambda\frac{\partial^2 T}{\partial x^2} \tag{2.29}$$

Both $\frac{\partial T}{\partial x}$ and $v_x\frac{\partial T}{\partial x}$ are negligible

Equation (2.21) becomes

$$c_p.\rho\left[-\lambda\frac{\partial^2 T}{\partial x^2}\right]=v_x\frac{\partial \Delta C}{\partial x} \tag{2.30}$$

Velocity of Self-Propagation

Based on eq. (2.30) and (2.15), we can derive the rate of reaction.

If we assume that ΔC is a linear function of C as shown in fig (2.2).

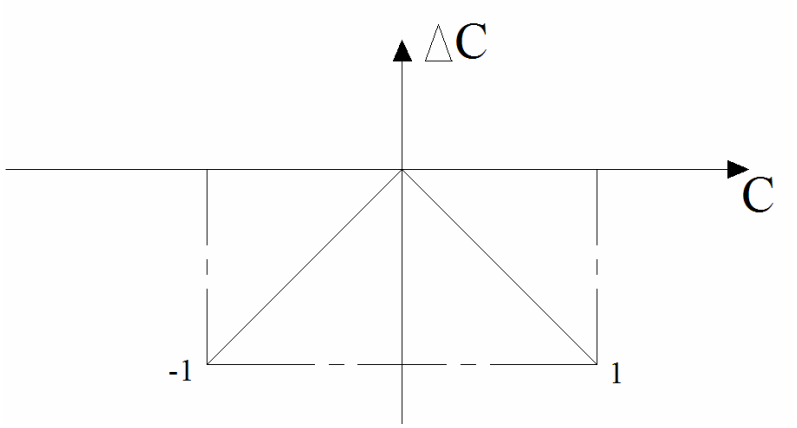

Figure 2-2 : Linear function of C

$$\Delta C = c_p . \rho . (T_f - T_0) C$$

Then the reaction rate:

$$v_x^{\,2} = \left(\sum_{n=odd} k_n / \alpha_n^{\,3} \right)^{-1} \frac{\lambda^2 R T_f^{\,2} A \delta}{E(T_f - T_0)} e^{\left(\frac{-E}{RT}\right)} \qquad (2.31)$$

b) If we assume that ΔC is a function of C^2 as shown in fig (2.3).

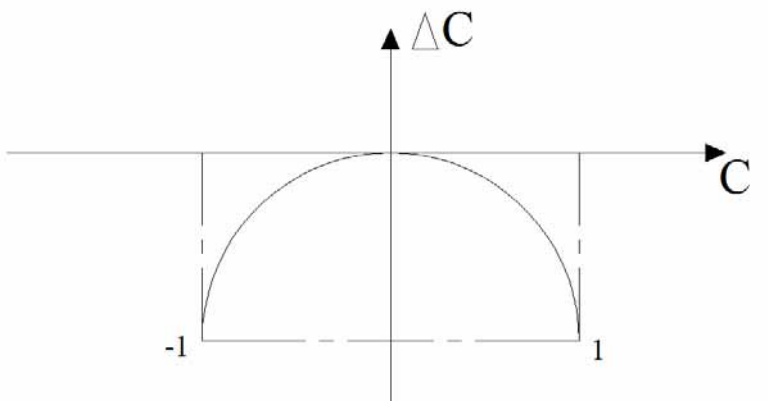

Figure 2-3 : Non-Linear Function of C

$$\Delta C = c_p . \rho . (T_f - T_0) C^2$$

Then the reaction rate:

$$v^2{}_x = \left(\sum_{n=odd} {k_n}^2 \Big/ {\alpha_n}^2 \right)^{-1} \frac{4\lambda^2 R {T_f}^2 A}{E\left(T_f - T_0\right)} e^{\left(\frac{-E}{RT}\right)} \tag{2.32}$$

In this analysis, we will use the linear profile as given in eq. (2.31).

Velocity of Self-Propagation CuO_x and Al

For a thin film of two material eq. (2.31) can be written as

$$v^2 = \frac{3\lambda D\left(\frac{RT_f}{E}\right)}{\delta^2\left(T_f - \frac{T_0}{T_f}\right)} e^{\left(\frac{-E}{RT_f}\right)} \tag{2.33}$$

Activation Energy of Multilayer Thin Film of Aluminum and Copper Oxide

Activation energy based on two typical speeds of propagation was calculated. In order to define the activation energy of a one-dimensional model, two speeds of propagation are measured by high-speed photograph technique:

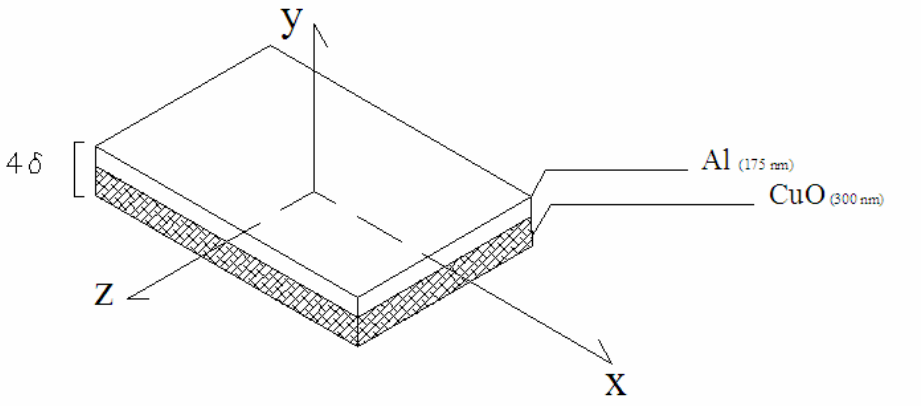

Figure 2-4 : Thin film Al/ CuO

λ	Thermal diffusion coefficient:	7.42 e-5 $m^2 s^{-1}$
D	Atomic diffusion coefficient (850 c):	6.4 e-5 $m^2 s^{-1}$
A	Arrhenius constant:	0.2
R	Ideal gas constant :	8.314 KJ/ kmol K
C_p	specific heat:	663 $Jkg^{-1} K^{-1}$
ρ	Density of the mixture:	5930 kg m^3
T_f	Final Temperature:	2846 K
T_0	Initial Temperature:	300 K
δ	diffusion length (¼ of the bi-layer of thin film):	133.75 nm
v	propagation velocity of the reaction	
T	temperature over interface line	

Calculation of Activation Energy (E)

- Total 20- repeating unit energetic material was used.
- The repeating unit : 175 nm aluminum
  300 copper oxide
  20 nm copper
- The kinetic reaction rate of a 20-repeating unit energetic film deposited onto the silicon wafer substrate is approximately 6.1 m/s
- The kinetic reaction rate a free (not deposited onto any substrate) energetic film is approximately 61 m/s
- Based on rate of reaction for multilayers (31)

$$v_x^{\,2} = \left(\sum_{n=odd} k_n \Big/ \alpha_n^{\,3} \right)^{-1} \frac{\lambda^2 R T_f^{\,2} A \delta}{E\left(T_f - T_0\right)} e^{\left(\frac{-E}{RT}\right)} \tag{2.31}$$

Number of layers, n=20

Using equations (2.16) and (2.17),

$$\alpha_n = n\pi \Big/ 2\delta \qquad\qquad k_n = 1 \Big/ 2\delta \int_{-2\delta}^{2\delta} C_0(y) \sin(\alpha_n y) dy \tag{2.34}$$

$$k_n = 1 \Big/ 2\delta \left(\int_{-2\delta}^{0} -\sin(\alpha_n y) dy + \int_{0}^{2\delta} \sin(\alpha_n y) dy \right) \tag{2.35}$$

Table 2-1 : Fourier Coefficients

n	1	3	5	7	9	11	13	15	17	19
α_n	$\pi/2\delta$	$3\pi/2\delta$	$5\pi/2\delta$	$7\pi/2\delta$	$9\pi/2\delta$	$11\pi/2\delta$	$13\pi/2\delta$	$15\pi/2\delta$	$17\pi/2\delta$	$19\pi/2\delta$
k_n	$4/\pi$	$4/3\pi$	$4/5\pi$	$4/7\pi$	$4/9\pi$	$4/11\pi$	$4/13\pi$	$4/15\pi$	$4/17\pi$	$4/19\pi$

$v_{\min} = 6.1 m/s$

Substituting for v_{min} in eq. (2.31) $\qquad E = 159.4\ kJ/mol$

$v_{\max} = 61 m/s$

Substituting for v_{max} in eq. (2.31) $\qquad E = 68.31\ kJ/mol$

The activation energy is calculated as $E = 68.3 - 159.4$ kJ/mole from existing measurements of v_{min} and v_{max} [37]. This compares well with the experimental rate of reaction for the CuO_x reaction for multilayer foils. CuO_x /Al multilayer foils were magnetron sputter deposited with ultrahigh purity Ar (5 Torr) onto silicon wafer substrates that were rotated above the CuO

(99.8%) and Al (99.99%) targets. The CuO target was RF sputtered at 200W and was DC sputtered at 150 W. The base pressure of the chamber was 1.9e-7 Torr. Each bilayer is 1 μ m and the first and last bi-layers are 0.5 μ m. The total foil thickness is 14 μ m. Self-propagating reaction was observed in these CuO_x /Al foils. Propagation velocity was 1 m/s. Based on their analysis, [1] proposed that the activation energy for the CuO_x/Al reaction lies between 146 and 460 KJ/mol. Therefore, in the current analysis, the calculated activation energy of $E = 68.3 - 159.4$ KJ/mol is in the same neighborhood, although this range is lower than that proposed by the Weihs' group [32].

Reaction Rate Profile Based on a Single Pair of Al and CuO

The reaction rate for a single pair thin film is given in eq. (2.33). This equation can be used to calculate the maximum and minimum velocity corresponding to the two extreme values of activation energy. This is shown in Figure 5.

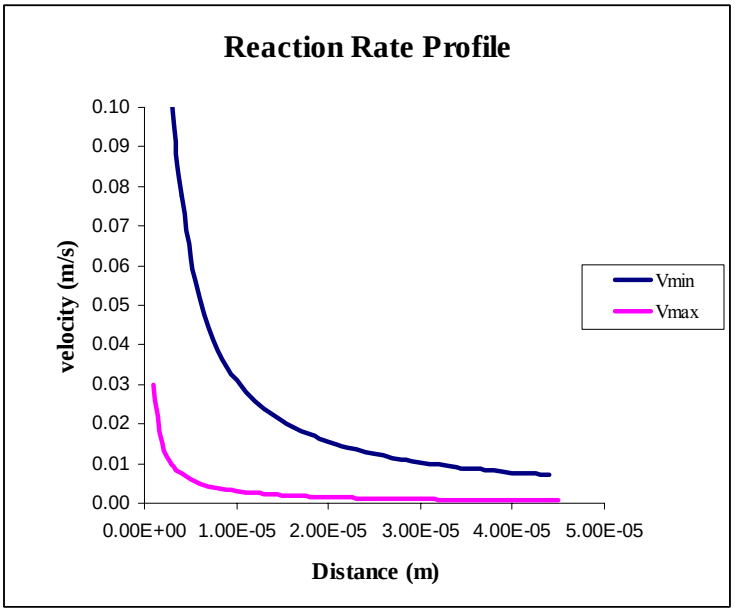

Figure 2-5 : Reaction Rate Profile as a Function of Thin Film, δ

$$v_{max}{}^2 = \frac{9.627*10^{-14}}{\delta^2} \qquad v_{min}{}^2 = \frac{8.995*10^{-16}}{\delta^2}$$

For δ =133.75 nm

$v_{min} = 0.2242$ m/s $\qquad v_{max} = 2.319$ m/s

Temperature Profile

Substituting velocity in eq. (2.30)

$$T = T_0 + \frac{v_x \cdot x}{c_p \cdot \rho \cdot \lambda} \Delta C \tag{2.36}$$

$$\Delta C = c_p \cdot \rho (T_f - T_0) C \tag{2.37}$$

For δ =133.75 nm $\quad v_{min} = 0.2242$ m/s $\qquad v_{max} = 2.319$ m/s

$T_{min}(x) = 300 + 7.68 \times 10^6 (x)$ and $T_{max}(x) = 300 + 7.957 \times 10^7 (x)$

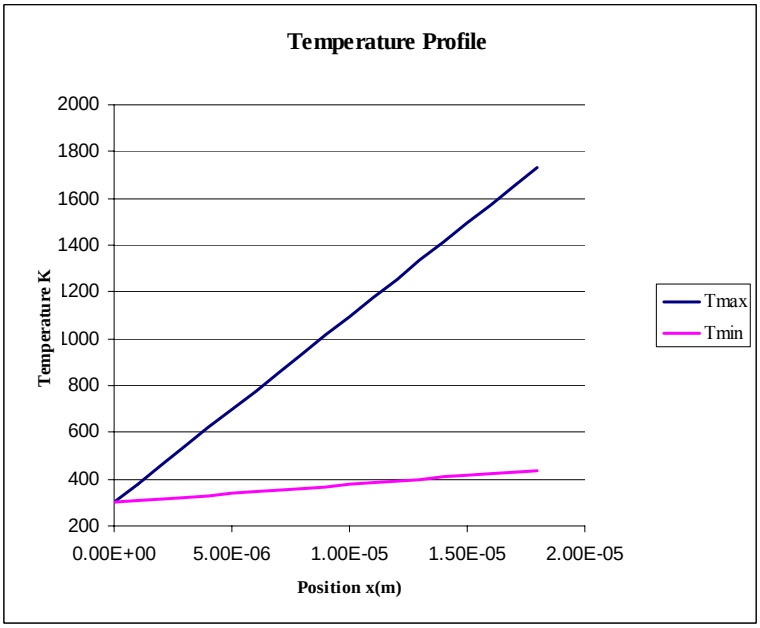

Figure 2-6 : Temperature Profile for one Pair Thin Film Al/CuO

As shown in Fig. 2.6, the temperature rises in the direction of propagation; however, the profile is linear and rises monotonically with distance. These fundamental flaws in the model were not previously exposed. This example shows approximately 100 kJ/mole difference for the lower and higher speeds of propagation. This large margin of error is an outcome of the model itself and is not reliable. In addition, the temperature variable, which is used in the Arrhenius type of equations, is the temperature at the critical point of the reaction, when combustion occurs. In self-propagation reaction, this temperature is one of the main unknown variables. In the solution of the problem used in the current method, the critical temperature is assumed to be 850^{o}C based on the reaction of Al/CuO in the bulk geometry as given by [32]. Another weakness of this model is that the speed of propagation is independent of the individual thicknesses of CuO and Al. Experimental data does not support this theory in Al/CuO reaction.

Summary of the One-Dimensional Model

In thin film geometry, a one-dimensional model for the speed of propagation in a multilayer thin film was discussed. In addition, two experimental speeds of propagation (minimum and maximum) were used to calculate the activation energy within scope of the model. Various possibilities for activation energy diminish the value of this model for the high speed of propagation reaction. Experimental data obtained recently with different levels of complexity are not validated due to the simplicity of this model. Therefore, it is necessary to develop a model that is more general, and will satisfy majority of the experimental data.

CHAPTER 3
PHASE TRANSFORMATION IN ADIABATIC UNIT CELL OF ALUMINUM AND COPPER OXIDE

MIC reactions create an enormous amount of energy, which causes phase transformation throughout the reaction. For the purpose of theoretical calculations, the scope and size of the process has been limited. The physical surface area in this study is limited to a cross section of a rectangular prism. Total amount of heat and final temperature of unit cell are calculated based on conservation of mass and energy.

Based on a review of various experiments, Fischer and Grubelich [33] proposed the energy release of the reaction aluminum and copper oxide to be 974.1 cal/g. Reaction starts in solid-solid phase, continues to liquid state, and finally ends in gas phase. Based on melting and boiling point of each one of the reactants and products, reaction of aluminum and copper oxide is broken into 6 different stages, as given in Table 3.1.

Table 3-1 : Six Different Stages for the Unit Cell Temperature

Temperature range (K)		**Effect at the end of process**
Start	**End**	
300	**933**	**Al Melts**
933	**1356**	**CuO Melts**
1356	**1358**	**Cu Melts**
1358	**2325**	**Al_2O_3 Melts**
2325	**2723**	**Al Vaporizes**
2723	**2793**	**Cu Vaporizes**

Description of the Method

In this part, the focus is on the reaction process in a very small area of two layers of Aluminum and copper oxide reaction surface. The cross section is chosen as a square unit, and the height is the sum of half of the two layers as shown in Figures 3.1 and 3.2. Based on the conservation of mass and energy principles, the proportional mass fraction of each reactant and the final product is calculated at each critical point and their physical state is verified.

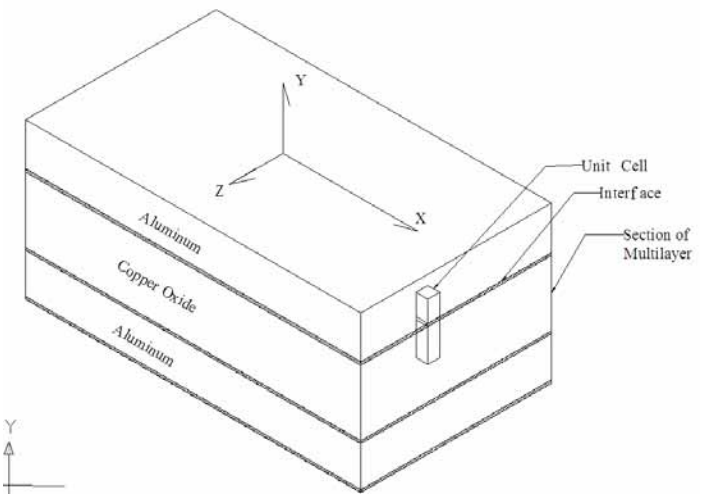

Figure 3-1 : Section of Multilayer

For the purpose of the theoretical calculations, the following assumptions have been made.

- Reactions are adiabatic.
- Variations in physical property of materials are linear between each critical point.
- Volumetric change of each reactant and the product are negligible.

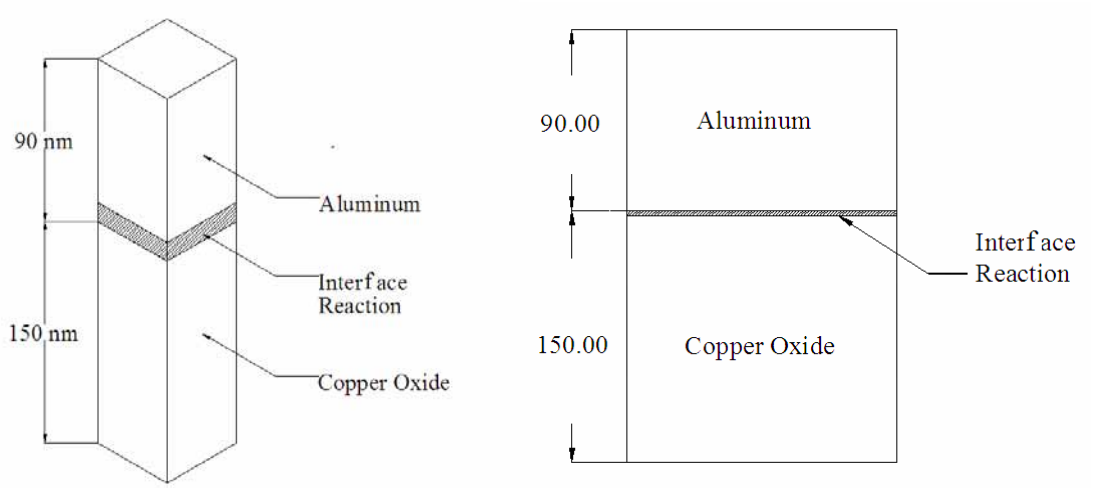

Figure 3-2 : Unit Volume Cell

Mass Conservation

At any stage of the chemical reaction, total mass is constant, so the mass of reactants is equal to the mass of the products. In this case, the total mass of aluminum and copper oxide are destroyed in each stage in the amount equal to the total mass of alumina and copper that is created.

$$2Al + 3CuO \rightarrow Al_2O_3 + 3Cu$$

$$m = \sum m_{Al} + m_{cuo} = \sum m_{Al_2O_3} + \sum m_{Cu} \tag{3.1}$$

Mass Ratio of Reactants and Product

Based on the atomic mass of the each reactant and product, the percentage of consumption and production of each material is calculated.

$$2Al + 3CuO \rightarrow Al_2O_3 + 3Cu$$

$$2M_{Al} + 3M_{CuO} \rightarrow M_{Al_2o_3} + 3M_{Cu}$$

For ‘m’ grams of reactants

$$100\frac{2M_{Al}}{2M_{Al}+3M_{Cuo}}(m)+100\frac{3M_{CuO}}{2M_{Al}+3M_{CuO}}(m)\rightarrow$$
$$100\frac{M_{Al_2o_3}}{M_{Al_2O3}+3M_{Cu}}(m)+100\frac{3M_{Cu}}{M_{Al_2O_3}+M_{Cu}}(m) \quad (3.2)$$

M_{Al} =26.98 g (based on periodic table of elements)

M_{Cu} =63.55g (based on periodic table of elements)

M_{O} =15.99 g (based on periodic table of elements)

$M_{Al_2O_3}$ =101.93 g

M_{CuO} =79.54 g

Reactant ratio : 81.55% m (CuO) + 18.45% m (Al) (3.3)

Product ratio : 34.84% m (Al_2O_3) + 65.15% m (Cu) (3.4)

Energy Conservation

Based on adiabatic assumption for reaction in each unit cell, energy balance follows the general rule.

$E_{IN} - E_{OUT} + E_{GEN} = E_{STOR}$ (3.5)

Energy Input (E_{IN}) and Output (E_{OUT})

Based on the initial assumption, heat generation in each volume cell is the same as the surrounding cells, so energy of input and output is zero.

Energy Generation (E GEN)

Based on the chemical reaction rate [33], energy released from chemical reaction of aluminum and copper oxide is 974.1cal/g

Energy Stored (E_{Stored})

Stored energy in each volume cell can change the temperature of the cell or change the physical state of the material. Energy released from the reaction is equal to the product of the specific heat at constant pressure and the change in the temperature of the system or change in the physical state of the reactants or product of the reaction. The properties required at each stage of the reaction are given in the tables in Appendix A[39].

Step 1.

Due to reaction of aluminum and copper oxide, Temperature of the system was raised from 300K to 933K; the melting point of aluminum.

$$(m_{Al}-m_{Al_{react}})\cdot C_{p_{Al}}\cdot(T_F-T_0)+(m_{CuO}-m_{CuO_{react}})\cdot C_{P_{CuO}}\cdot(T_F-T_0)+m_{Al_2O_3}\cdot C_{P_{Al_2O_3}}\cdot(T_F-T_0)+ m_{Cu}\cdot C_{P_{Cu}}\cdot(T_F-T_0)=\Delta H_{Al+CuO}\cdot(m_{Al}+m_{CuO}) \quad (3.6)$$

$m_{Al}=V_{Al}\cdot\rho_{Al}=946.5\times10^{-9}$ g (from Figure 3.2)

$m_{CuO}=V_{CuO}\cdot\rho_{CuO}=243.18\times10^{-9}$ g (from Figure 3.2)

From eq. (3.3),

$m_{Al\,react}=18.45\%m$ $m_{CuO\,react}=81.55\%m$

From eq. (3.4),

$m_{Al2o3}=34.85\%m$ $m_{Cu}=65.15\%m$

T_0=300K T_F=933K

$$C_p = \frac{C_{P@300K} + C_{P@933K}}{2}$$

$C_{p_{Al}} = 0.903$ kJ/kg.K, $C_{p_{Cu}} = 0.385$ kJ/kg.K

$C_{p_{Cuo}} = 0.6455$ kJ/kg.K, $C_{p_{AL2O3}} = 0.9996$ kJ/kg.K

$\Delta H_{Al+CuO} = 947.1\ cal/gr$

From eq. (3.6),

$$(946.5\times10^{-9} - 0.8155m_1)\cdot C_{PCuO}\cdot(T_F - T_0) + (243.18\times10^{-9} - 0.1845m_1)\cdot C_{PAl}\cdot(T_F - T_0) + 0.3485\cdot m_1\cdot C_{P_{Al_2O_3}}\cdot(T_F - T_0) + 0.6515\cdot m_1\cdot C_{P_{Cu}}\cdot(T_F - T_0) = \Delta H_{Al+CuO}\cdot m_1$$

Solve for m_1 $\quad m_1 = 126.695\times10^{-9}$ g

$m = \sum m_n = 126.695\times10^{-9}$ g

Table 3-2 : Products and Reactants after Step 1

m $\times10^{-9}$ g	Al m $\times10^{-9}$ g	CuO m $\times10^{-9}$ g	Al2O3 m$\times10^{-9}$ g	Cu m $\times10^{-9}$ g
126.695	219.763	843.18	44.14	82.54

Step 2.

Due to the reaction of aluminum and copper oxide, aluminum melts at 933K.

$$(m_{Al})\cdot\Delta H_{Al_{melting}} = \Delta H_{Al+CuO}\cdot(m_{Al} + m_{CuO}) \qquad (3.7)$$

$m_{Al} = 219.76\times10^{-9}$ g (table 3.2)

$\Delta H_{Al_{melting}} = 94.8$ cal/g

$$(219.763)\cdot\Delta H_{Al_{melting}} = \Delta H_{Al+CuO}\cdot m_2$$

Solve for m_2 $m_2 = 21.9 \times 10^{-9}$ g

$m = \sum m_n = 147.695 \times 10^{-9}$ g

Table 3-3 : Products and Reactants after Step 2

$m \times 10^{-9}$ g	Al $m \times 10^{-9}$ g	CuO m $\times 10^{-9}$ g	Al2O3 $m \times 10^{-9}$ g	Cu $m \times 10^{-9}$ g
147.695	215.888	826.055	56.715	90.906

Step 3

Due to reaction of aluminum and copper oxide, Temperature of the system was raised from 933K to 1356K melting point of copper oxide.

Follow similar process in step1:

$$(m_{Al} - m_{Al_{react}}) \cdot C_{p_{Al}} \cdot (T_F - T_0) + (m_{CuO} - m_{CuO_{react}}) \cdot C_{P_{CuO}} \cdot (T_F - T_0) + m_{Al_2o_3} \cdot C_{P_{Al_2O_3}} \cdot (T_F - T_0) + m_{Cu} \cdot C_{P_{Cu}} \cdot (T_F - T_0) = \Delta H_{Al+CuO} \cdot (m_{Al} + m_{CuO}) \quad (3.6)$$

T_0=933K T_F=1356K

$m_{Al} = 215.88 \times 10^{-9}$ g (table-3.3)

$m_{CuO} = 826.055 \times 10^{-9}$ g (table-3.3)

$C_{p_{Al}} = 0.903$ kJ/kg.K, $C_{p_{Cu}} = 0.385$ kJ/kg.K

$C_{p_{Cuo}} = 0.7665$ kJ/kg.K, $C_{p_{AL2O3}} = 1.2847$ kJ/kg.K

$\Delta H_{Al+CuO} = 947.1$ cal/g

$$(826.055 \times 10^{-9} - 0.8155 m_3) \cdot C_{p_{CuO}} \cdot (T_F - T_0) + (215.88 \times 10^{-9} - 0.1845 m_3) \cdot C_{P_{Al}} \cdot (T_F - T_0) + 0.3485 \cdot m_3 \cdot C_{P_{Al_2O_3}} \cdot (T_F - T_0) + 0.6515 \cdot m_3 \cdot C_{P_{Cu}} \cdot (T_F - T_0) = \Delta H_{Al+CuO} \cdot m_3$$

Solve for m_3 $m_3 = 85.968 \times 10^{-9}$ g

$$m = \sum m_n = 233.66 \times 10^{-9} \text{ g}$$

Table 3-4 : Products and Reactants after Step 3

m $\times 10^{-9}$ g	Al m $\times 10^{-9}$ g	CuO m $\times 10^{-9}$ g	Al2O3 m$\times 10^{-9}$ g	Cu m $\times 10^{-9}$ g
2.33.66	200.027	755.94	81.408	152.231

Step 4.

Due to the reaction of aluminum and copper oxide, copper oxide melts at 1056K.

Follow similar process in step 2:

$$(m_{CuO} - m_{CuO_{react}}) \cdot \Delta H_{cuo_{melting}} = \Delta H_{Al+CuO} \cdot (m_{Al} + m_{CuO}) \quad (3.8)$$

$$(m_{Al}) \cdot \Delta H_{Al_{melting}} = \Delta H_{Al+CuO} \cdot (m_{Al} + m_{CuO})$$

$m_{CuO} = 755.94 \times 10^{-9}$ g (table -3.4)

$\Delta H_{CuO_{melting}} = 35.4$ cal/g

$$(m_{cuo}) \cdot \Delta H_{CuO_{melting}} = \Delta H_{Al+CuO} \cdot m4$$

Solve for m_4 $m_4 = 27.47 \times 10^{-9}$ g

$$m = \sum m_n = 261.135 \times 10^{-9} \text{g}$$

Table 3-5 : Products and Reactants after Step 4

m $\times 10^{-9}$ g	Al m $\times 10^{-9}$ g	CuO m $\times 10^{-9}$ g	Al2O3 m$\times 10^{-9}$ g	Cu m $\times 10^{-9}$ g
261.135	194.95	733.544	90.979	170.129

Step 5.

Due to reaction of aluminum and copper oxide, Temperature of the system was raised from 1356 K to 1358 K melting point of copper.

Follow similar process in step 1:

$$(m_{Al} - m_{Al_{react}}) \cdot C_{p_{Al}} \cdot (T_F - T_0) + (m_{CuO} - m_{CuO_{react}}) \cdot C_{P_{CuO}} \cdot (T_F - T_0) + m_{Al_2O_3} \cdot C_{P_{Al_2O_3}} \cdot (T_F - T_0) + m_{Cu} \cdot C_{P_{Cu}} \cdot (T_F - T_0) = \Delta H_{Al+CuO} \cdot (m_{Al} + m_{CuO})$$ T_0

=1356 K T_F=1358 K

$m_{Al} = 194.95 \times 10^{-9}$ g (table-3.5)

$m_{CuO} = 733.544 \times 10^{-9}$ g (table-3.5)

$C_{p_{Al}} = 0.903$ kJ/kg.K, $C_{p_{Cu}} = 0.385$ kJ/kg.K

$C_{p_{Cuo}} = 0.7665$ kJ/kg.K, $C_{p_{AL2O3}} = 1.2847$ kJ/kg.K

$\Delta H_{Al+CuO} = 947.1$ cal/g

$$(733.54 \times 10^{-9} - 0.8155 m_5) \cdot C_{p_{CuO}} \cdot (T_F - T_0) + (194.95 \times 10^{-9} - 0.1845 m_5) \cdot C_{P_{Al}} \cdot (T_F - T_0) + 0.3485 \cdot m_5 \cdot C_{P_{Al_2O_3}} \cdot (T_F - T_0) + 0.6515 \cdot m_5 \cdot C_{P_{Cu}} \cdot (T_F - T_0) = \Delta H_{Al+CuO} \cdot m_5$$

Solve for m_5 $m_5 = 0.3609 \times 10^{-9}$ g

$m = \sum m_n = 261.496 \times 10^{-9}$ g

Table 3-6 : Products and Reactants after Step 5

m $\times 10^{-9}$ g	Al m $\times 10^{-9}$ g	CuO m $\times 10^{-9}$ g	Al2O3 m$\times 10^{-9}$ g	Cu m $\times 10^{-9}$ g
261.496	194.892	733.25	91.105	170.365

Step 6.

Due to reaction of aluminum and copper oxide, copper is melting at 1358K.

Follow similar process in step2:

$$(m_{cu} - m_{cu_{react}}) \cdot \Delta H_{cu_{melting}} = \Delta H_{Al+CuO} \cdot (m_{Al} + m_{CuO}) \tag{3.9}$$

$m_{Cu} = 219.76 \times 10^{-9}$ g (table -3.6)

$\Delta H_{Cu_{melting}} = 32$ cal/g

$(170.365) \cdot \Delta H_{Cu_{melting}} = \Delta H_{Al+CuO} \cdot m_6$

Solve for m_6 $m_6 = 5.597 \times 10^{-9}$ g

$m = \sum m_n = 267.093 \times 10^{-9}$ g

Table 3-7 : Products and Reactants after Step 6

m $\times 10^{-9}$ g	Al m $\times 10^{-9}$ g	CuO m $\times 10^{-9}$ g	Al2O3 m$\times 10^{-9}$ g	Cu m $\times 10^{-9}$ g
267.093	193.059	728.686	93.0552	174.011

Step 7.

Due to reaction of aluminum and copper oxide, Temperature of the system was raised from 1358 k to 2325k melting point of alumina (Al_2O_3).

Follow similar process in step 1:

$$(m_{Al} - m_{Al_{react}}) \cdot C_{p_{Al}} \cdot (T_F - T_0) + (m_{CuO} - m_{CuO_{react}}) \cdot C_{P_{CuO}} \cdot (T_F - T_0) + m_{Al_2o_3} \cdot C_{P_{Al_2O_3}} \cdot (T_F - T_0) + m_{Cu} \cdot C_{P_{Cu}} \cdot (T_F - T_0) = \Delta H_{Al+CuO} \cdot (m_{Al} + m_{CuO}) \tag{6}$$

T_0=1358 K T_F=2325 K

$m_{Al} = 193.059 \times 10^{-9}$ g (table-3.7)

$m_{CuO} = = 728.686 \times 10^{-9}$ g (table-3.7)

$C_{p_{Al}} = 0.903$ kJ/kg.K, $C_{p_{Cu}} = 0.385$ kJ/kg.K

$C_{p_{Cuo}} = 0.8064$ kJ/kg.K, $C_{p_{AL2O3}} = 1.344$ kJ/kg.K

$\Delta H_{Al+CuO} = 947.1$ cal/g

$(728.686 \times 10^{-9} - 0.8155 m_7) \cdot C_{p_{CuO}} \cdot (T_F - T_0) + (193.059 \times 10^{-9} - 0.1845 m_7) \cdot C_{P_{Al}} \cdot (T_F - T_0) + 0.3485 \cdot m_7 \cdot C_{P_{Al_2O_3}} \cdot (T_F - T_0) + 0.6515 \cdot m_7 \cdot C_{P_{Cu}} \cdot (T_F - T_0) = \Delta H_{Al+CuO} \cdot m_7$ Solv

e for m_7 $m_7 = 176.091 \times 10^{-9}$ g

$m = \sum m_n = 443.184 \times 10^{-9}$ g

Table 3-8 : Products and Reactants after Step 7

m $\times 10^{-9}$ g	Al m $\times 10^{-9}$ g	CuO m $\times 10^{-9}$ g	Al2O3 m$\times 10^{-9}$ g	Cu m $\times 10^{-9}$ g
443.184	161.371	585.083	154.405	288.734

Step 8.

Due to reaction of aluminum and copper oxide, alumina is melting at 2325K.

Follow similar process in step2:

$(m_{Al2O3}) \cdot \Delta H_{Al2o3_{melting}} = \Delta H_{Al+CuO} \cdot (m_{Al} + m_{CuO})$ (3.10)

$m_{Al2o3} = 154.405 \times 10^{-9}$ g (table -3.8)

$\Delta H_{Al2o3_{melting}} = 250.646$ cal/g

$(m_{Al2O3}) \cdot \Delta H_{Al2O3_{melting}} = \Delta H_{Al+CuO} \cdot m_8$

Solve for m_8 $m_8 = 39.734 \times 10^{-9}$ g

$m = \sum m_n = 482.918 \times 10^{-9}$ g

Table 3-9 : Products and Reactants after Step 8

m $\times 10^{-9}$ g	Al m $\times 10^{-9}$ g	CuO m $\times 10^{-9}$ g	Al2O3 m$\times 10^{-9}$ g	Cu m $\times 10^{-9}$ g
482.918	154.04	552.68	168.249	314.621

Step 9.

Due to reaction of aluminum and copper oxide, Temperature of the system was raised from 2325K to 2723K, which is the vaporizing point of aluminum.

Follow similar process in step1:

$$(728.686\times10^{-9} - 0.8155m_7)\cdot C_{p_{CuO}}\cdot(T_F - T_0) + (193.059\times10^{-9} - 0.1845m_7)\cdot C_{P_{Al}}\cdot(T_F - T_0) + 0.3485\cdot m_7\cdot C_{P_{Al_2O_3}}\cdot(T_F - T_0) + 0.6515\cdot m_7\cdot C_{P_{Cu}}\cdot(T_F - T_0) = \Delta H_{Al+CuO}\cdot m_7 \quad (3.6)$$

T_0=2325 K T_F=2723 K

$m_{Al} = 154.04\times10^{-9}$ g (table-3.9)

$m_{CuO} = 215.888\times10^{-9}$ g (table-3.9)

$C_{p_{Al}} = 0.903$ kJ/kg.K, $C_{p_{Cu}} = 0.385$ kJ/kg.K

$C_{p_{Cuo}} = 0.8064$ kJ/kg.K, $C_{p_{AL2O3}} = 1.344$ kJ/kg.K

$\Delta H_{Al+CuO} = 947.1$ cal/g

$$(552.68\times10^{-9} - 0.8155m_9)\cdot C_{p_{Al}}\cdot(T_F - T_0) + (154.04\times10^{-9} - 0.1845m_9)\cdot C_{P_{CuO}}\cdot(T_F - T_0) + 0.3485\cdot m_9\cdot C_{P_{Al_2O_3}}\cdot(T_F - T_0) + 0.6515\cdot m_9\cdot C_{P_{Cu}}\cdot(T_F - T_0) = \Delta H_{Al+CuO}\cdot m_9$$

Solve for m_9 $m_9 = 56.33 \times 10^{-9}$ g

$m = \sum m_n = 539.256 \times 10^{-9}$ g

Table 3-10 : Products and Reactants after Step 9

m $\times 10^{-9}$ g	Al m $\times 10^{-9}$ g	CuO m $\times 10^{-9}$ g	Al2O3 m $\times 10^{-9}$ g	Cu m $\times 10^{-9}$ g
539.256	143.645	506.737	187.8774	351.325

Step 10.

Due to reaction of aluminum and copper oxide, aluminum is vaporized at 2723 k

Follow similar process in step 2:

$$(m_{Al} - m_{Al_{react}}) \cdot \Delta H_{Al_{vap}} = \Delta H_{Al+CuO} \cdot (m_{Al} + m_{CuO}) \quad (3.11)$$

$(m_{Al}) \cdot \Delta H_{Alvap} = \Delta H_{Al+CuO} \cdot (m_{10})$

$m_{Al} = 143.64 \times 10^{-9}$ g (table -3.10)

$\Delta H_{Al_{vap}} = 2720$ cal/g

$(m_{Al}) \cdot \Delta H_{Al_{vap}} = \Delta H_{Al+CuO} \cdot m_{10}$

Solve for m_{10} $m_{10} = 401.144 \times 10^{-9}$ g

$m = \sum m_n = 940.4 \times 10^{-9}$

Table 3-11 : Products and Reactants after Step 10

m $\times 10^{-9}$ g	Al m $\times 10^{-9}$ g	CuO m $\times 10^{-9}$ g	Al2O3 m $\times 10^{-9}$ g	Cu m $\times 10^{-9}$ g
940.4	69.634	179.604	327.635	612.671

Step 11.

Due to reaction of aluminum and copper oxide, Temperature of the system was raised from 2723 k to 2793 k vaporizing point of copper.

Follow similar process in step1:

$$(728.686\times10^{-9}-0.8155m_7)\cdot C_{p_{CuO}}\cdot(T_F-T_0)+(193.059\times10^{-9}-0.1845m_7)\cdot C_{P_{Al}}\cdot(T_F-T_0)+$$
$$0.3485\cdot m_7\cdot C_{P_{Al_2O_3}}\cdot(T_F-T_0)+0.6515\cdot m_7\cdot C_{P_{Cu}}\cdot(T_F-T_0)=\Delta H_{Al+CuO}\cdot m_7$$

T_0=2723 K T_F=2793 K

$m_{Al}=69.634\times10^{-9}$ g (table-3.11)

$m_{CuO}=179.0\times10^{-9}$ g (table-3.11)

$C_{p_{Al}}=0.903$ kJ/kg.K, $C_{p_{Cu}}=0.385$ kJ/kg.K

$C_{p_{Cuo}}=0.8064$ kJ/kg.K, $C_{p_{AL2O3}}=1.344$ kJ/kg.K

$\Delta H_{Al+CuO}=947.1$ cal/g

$$(69.634\times10^{-9}-0.8155m_{11})\cdot C_{p_{Al}}\cdot(T_F-T_0)+(179.604\times10^{-9}-0.1845m_{11})\cdot C_{P_{CuO}}\cdot(T_F-T_0)+$$
$$0.3485\cdot m_{11}\cdot C_{P_{Al_2O_3}}\cdot(T_F-T_0)+0.6515\cdot m_{11}\cdot C_{P_{Cu}}\cdot(T_F-T_0)=\Delta H_{Al+CuO}\cdot m_{11}$$

Solve for m_{11} $m_{11}=3.5478\times10^{-9}$ g

$m=\sum m_n=943.9478\times10^{-9}$ g

Table 3-12 : Products and Reactants after Step 11

m $\times10^{-9}$ g	Al m $\times10^{-9}$ g	CuO m $\times10^{-9}$ g	Al2O3 m$\times10^{-9}$ g	Cu m $\times10^{-9}$ g
943.94	68.979	176.711	328.87	615.076

Step 12.

Due to reaction of remainder of aluminum and copper oxide, 33% of copper is vaporized at 2793 K.

$$(m_{Cu_{vap}}) \cdot \Delta H_{Cu_{vap}} = \Delta H_{Al+CuO} \cdot (m_{Al} + m_{CuO}) \qquad (3.12)$$

$$m = \frac{176.711}{.08155} \text{ g} \qquad \text{(table -3.12)}$$

$$\Delta H_{Cu_{vap}} = 2793 \text{ cal/g}$$

$$(m_{Cu_{vap}}) \cdot \Delta H_{Al_{melting}} = \Delta H_{Al+CuO} \cdot m$$

Solve for m_{cu} $\quad m_{Cu} = 174.42 \times 10^{-9} \text{ g}$ $m_{cu_{vap}}\% = \frac{174.426}{756.15} = 23.06\%$ of copper vaporized

Table 3-13 : Products and Reactants after Step 12

m $\times 10^{-9}$ g	Al m $\times 10^{-9}$ g	CuO m $\times 10^{-9}$ g	Al2O3 m$\times 10^{-9}$ g	Cu m $\times 10^{-9}$ g
	28.9906	0	404.366	756.15

$$(m_{Al} - m_{Al_{react}}) \cdot \Delta H_{Al_{vaporizing}} = \Delta H_{Al+CuO} \cdot (m_{Al} + m_{CuO})$$

The reaction ends when the entire copper oxide is consumed. Table 3.13 shows the overall mass fraction of the reactants and product at each point of the physical state change. The percentage of the reactants and product is also given in figure 3.3.

Table 3-14 : Summary of Products and Reactants after each Step

Temperature	CuO $\times 10^{-9}$ (g)	Al $\times 10^{-9}$ (g)	Al2O3 $\times 10^{-9}$ (g)	Cu $\times 10^{-9}$ (g)	Reactant $\times 10^{-9}$ (g)	Product $\times 10^{-9}$ (g)
300	**946.5**	**243.138**	**0**	**0**	**1189.638**	**0**
933	**843.18**	**219.763**	**44.14**	**82.541**	**1062.943**	**126.681**
933	**826.055**	**215.888**	**56.714**	**90.906**	**1041.943**	**147.62**
1356	**755.94**	**200.027**	**81.408**	**152.231**	**955.967**	**233.639**
1356	**733.544**	**194.959**	**90.979**	**170.129**	**928.503**	**261.108**
1358	**733.25**	**194.892**	**91.105**	**170.365**	**928.142**	**261.47**
1358	**728.686**	**193.059**	**93.055**	**174.011**	**921.745**	**267.066**
2325	**585.083**	**161.371**	**154.405**	**288.734**	**746.454**	**443.139**
2325	**552.68**	**154.04**	**168.249**	**314.621**	**706.72**	**482.87**
2723	**506.737**	**143.645**	**187.877**	**351.325**	**650.382**	**539.202**
2723	**179.604**	**69.634**	**327.635**	**612.671**	**249.238**	**940.306**
2793	**176.711**	**68.979**	**328.87**	**615.076**	**245.69**	**943.946**
2793	**0**	**28.99**	**404.366**	**756.15**	**28.99**	**1160.516**

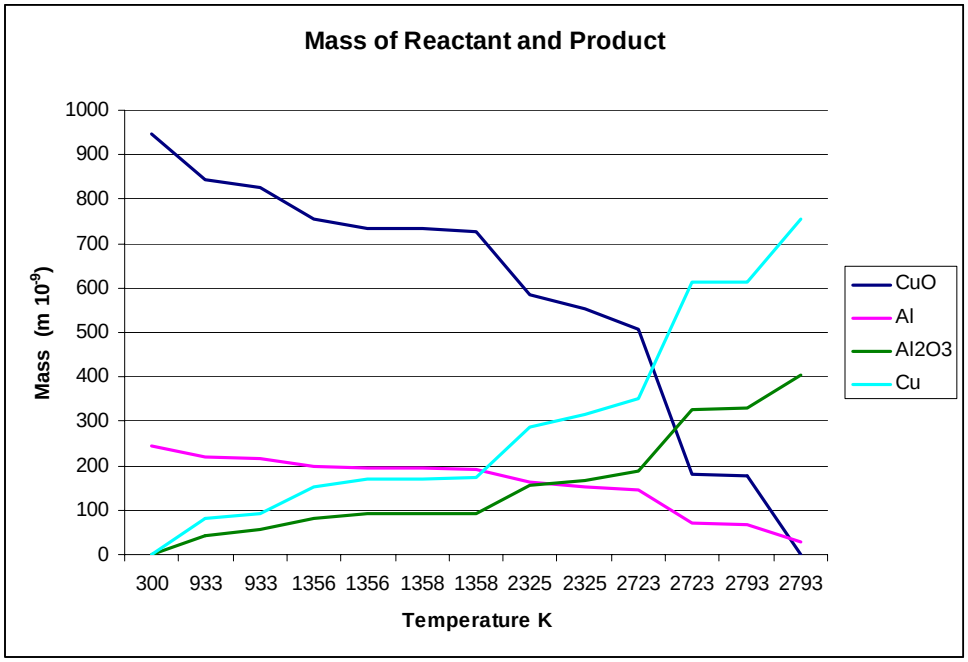

Figure 3-3 : Mass of the Reactants and Products as a function of temperature

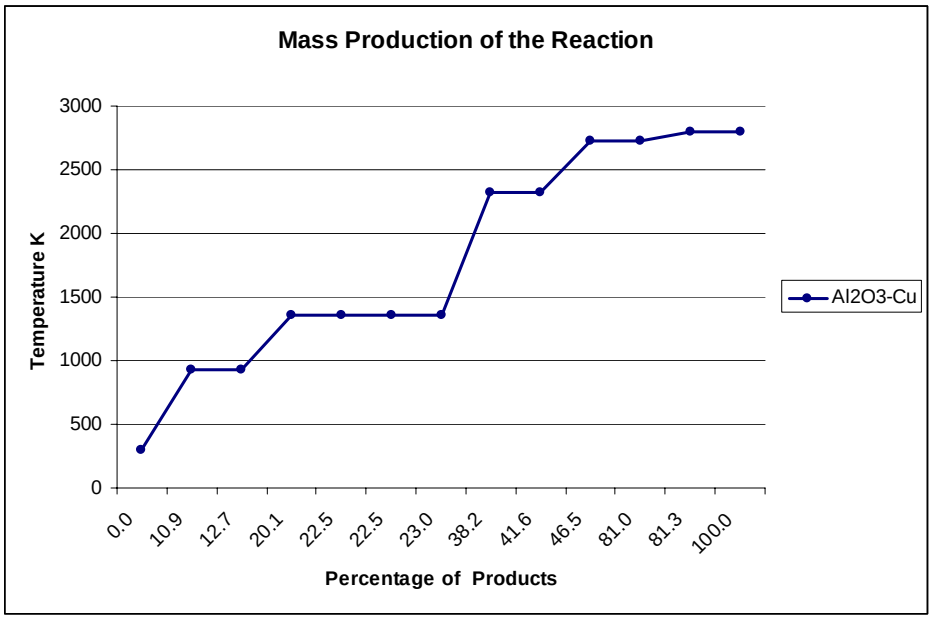

Figure 3-4 : Temperature vs. %mass of the products

Discussion

Figure 3.4 shows the mass of reactants and products at each stage of temperature range. Figure 3.5 shows the schematic and overall view of the reaction and phase change from 300K to 2793K. Before 933K, all the products and reactants are in solid phase and the reaction is based on diffusion in solid-solid phase. Between 933K to1356K, aluminum is changed to liquid phase and the reaction is based on diffusion in solid–liquid phase. Between 1358K and 2325 K reactants are in liquid phase and the reaction rate is based on the diffusion of liquid-liquid phase and subsequently much faster than before. At this stage, there is still alumina present in solid state and has a negative effect on the reaction rate. Between 2325K to2723K, all the products and reactants are in pure liquid phase and reaction rate is highest at this point. Above 2723K, reaction enters the gas phase of the reactants and the rate of reaction accelerates to its highest rate.

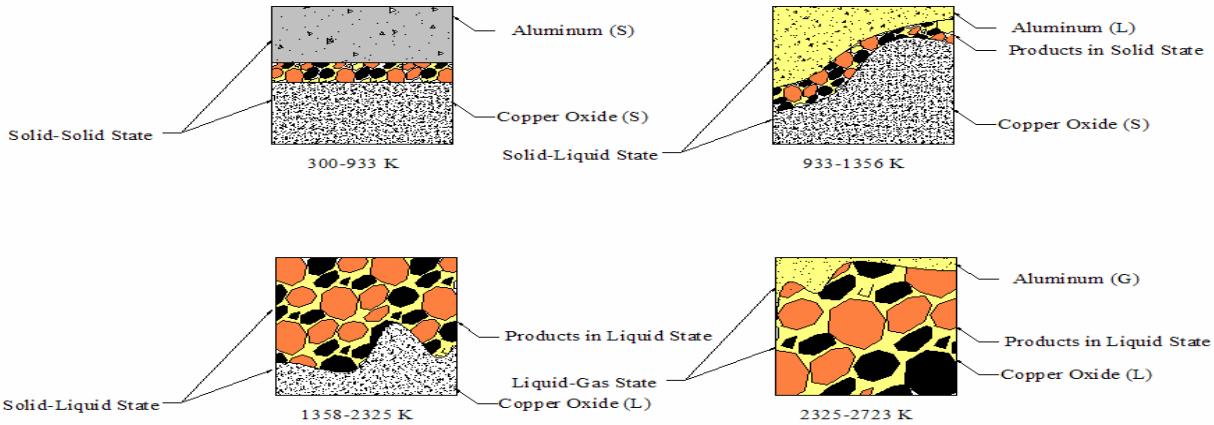

Figure 3-5 : Schematic of the Physical State of Reactants and Product in Different Range of Temperature

Figure 3.6 shows the final products of multilayer reaction of Al/CuO using a Scanning Electron Microscope. The image shows the copper particles are coalesced together within the alumina.

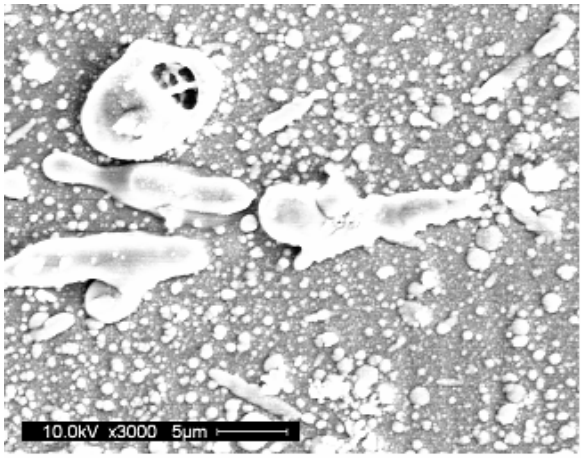

Figure 3-6 : Scanning Electron Micrograph of Reacted Layered MIC [10]

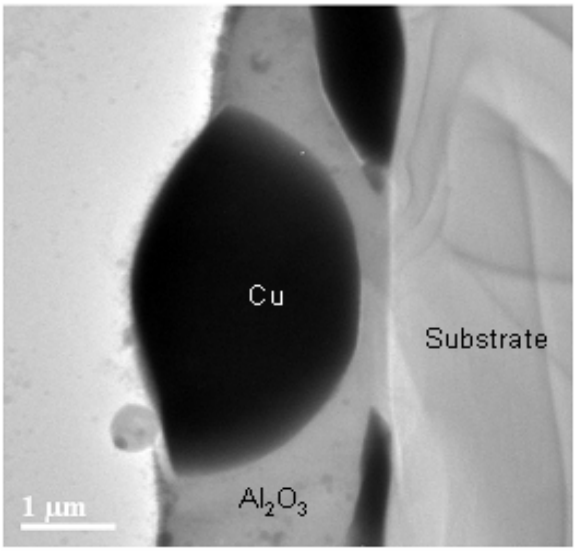

Figure 3-7 : Bright Field Transmission Electron Microscopy of the Cross Section of Reacted Layer of MIC [10]

More details can be seen from the products captured by transmission electron microscopy (TEM) in Figure 3.7. Copper with more dense structure is shown as a darker image with respect to alumina.

In this method, some the complexities of the process due to the phase transformation are captured. However, this method is seen to have some shortcomings. In order to simplify and isolate some of the variables, a one-dimensional model was used although the geometry of the multi-layer thin film dictates a two-dimensional analysis. In addition, unit cell is not treated here as a moving source, therefore, the concentration profile does not exist and the rate of reaction at the interface is constant. An average temperature profile at any point along the reaction is calculated in the model.

Summary of the Phase Transformation in an Adiabatic Cell

Conservation of mass and energy was used to demonstrate the reaction of aluminum and copper oxide in the adiabatic unit cell. Twelve different steps describe the process. While aluminum and copper oxide are being consumed, they are transformed from solid to liquid. The process generates copper and alumina in solid, liquid, and gas phases. Numerical solution shows that 2793±100K is the highest possible temperature for the reaction.

CHAPTER 4
EXPERIMENTAL AND NUMERICAL STUDY OF DENSE LAYERED NANO-ENERGETIC MATERIALS

Due to the complexity of the motion of the products during the reaction and the number of unknowns, one-dimensional models do not explain the overall physical phenomena. The process can be simplified without diffusion by the introduction of the black box theory in the combustion phenomena [39-40]. In this approach, control volume moves with the flame front so concentration profile need not be considered. The reactions within the black box are considered steady state and are not part of the calculations. The concept of the black box volume allows us to isolate the effects of the interaction of the control volume and the surroundings within the defined frame. The control volume is moving with the speed of propagation along the reaction path. The velocity of the control volume along the direction of propagation of the reaction is assumed constant.

The number of variables can affect the MIC reaction process. In order to measure and compare some of the characteristics of the flame, the number of variables needs to be reduced and some isolated during the experiments. By creating a standard geometry, some of the influencing variables may be eliminated, and a controlled environment can be created for consistent results in MIC reactions. Measuring some of the characteristics of the flame such as the speed of the flame front is one the main goals of this work. Although high-speed photography is one of the popular techniques for measurement of speed of propagation, accuracy of this technique is decreased significantly in high-speed propagation reactions, such as aluminum and copper oxide.

The main approach in this work is to identify and experimentally measure the characteristics and variables of the flame. This method can be helpful in understanding the propagation process, theoretically and experimentally. Thus, the goal is to obtain a greater physical understanding of the reaction process and to increase the reaction propagation velocity (burn rate) of dense MIC. The objective of this work is to use a combined approach, consisting of an experimental effort, supported by analytical and numerical modeling. To support the experimental effort, samples of Al/CuO has been prepared as multilayer thin film by vacuum deposition. The experimental effort is to study the kinetics of MIC reactions, using the reaction propagation velocity as a measure of the reaction process. This effort extends prior studies of propagation velocity as a function of the substrate thickness.

Reaction Model and Mechanism

For self-propagating (non-isothermal) MIC reactions, the melting of both the reactant layers and products during reaction requires consideration. The reaction temperature calculated during the course of the adiabatic reaction of Al/CuO multilayers is shown in Figure 4.1.

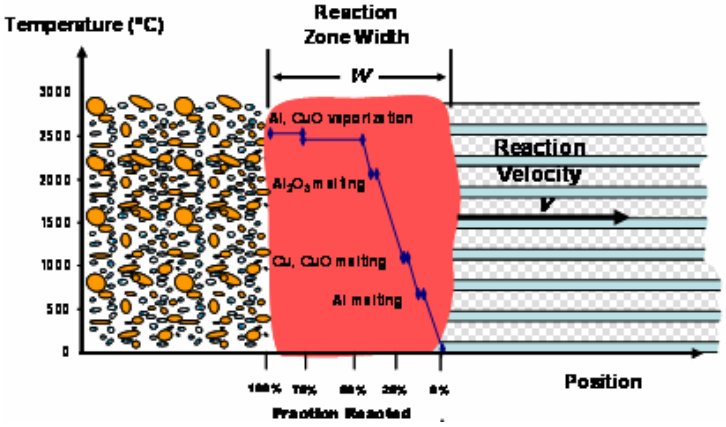

Figure 4-1 : Idealize View of Layered MIC Reaction Propagation

Significantly, we can expect both Al and CuO reactant layers and the Cu product layer to be molten before the reaction is 25% complete. The alumina product layers will also melt before the reaction reaches 50% completion. Liquid phase diffusion across the product layers and the direct liquid phase mixing of the reactant layers must be considered. Khina, et. al. [41] have suggested a reaction mechanism wherein the initially layered reactants form a homogeneous molten solution, from which the product phase precipitates. The vaporization of both reactants and the possibility of the decomposition of CuO introduce vapor phase reaction mechanisms as well. Thus, there are many possible ways MIC reactions can take place, occurring at sequentially higher temperatures. The key parameter that will help identify the rate-limiting mechanism is the temperature near which it occurs, i.e., the critical reaction temperature (T_c). The experimental determination of T_c is difficult, and therefore an idealized model given in Figure 4.2 is considered in order to obtain maximum temperature at the leading edge of the flame.

In Ni-Al layers, Zanotti et al. [42] divided the process into separate phases of initiation and self-propagation. Self-propagation is the focus of this study and can be independently researched. Ignition and initiation process can be neglected in part due to the work done by Zanotti et al. [42]. They established that the relative amount of energy of the ignition compared to the overall reaction is negligible. The calculations are focused on the period of self- propagation cycles.

Defining the speed of propagation, which is assumed to be the same as the speed of the product during the reaction process, is a major step toward modeling of the MIC reaction. In order to narrow the field of the variables, the concept of the black box theory is utilized. Figure 4.2 shows the general black box with simple input and output. The reactions within the black box are considered as steady state and are not part of the calculations. Concept of the control

volume allows us to study the effects of the interaction of the black box and the surroundings within the defined frame. The control volume (flame) is moving with the speed of propagation along the reaction process path. The process can be simplified as input, reaction and the output. Input can be identified as reactants and is a known variable. The reaction process can be simplified as conversion of input to heat and the product, which is the output. Heat increases the temperature based on a defined profile. The velocity of the control volume through the direction of flame propagation is assumed constant and is the same as the speed of the particles. Capability of measuring the speed of flame front or speed of propagation accurately can help calculate some of the effective variables of this process, such as length of flame, and rate of heat generation. The measurement of this speed of propagation is crucial to the calculation of temperature and the amount of heat dissipated into the substrates.

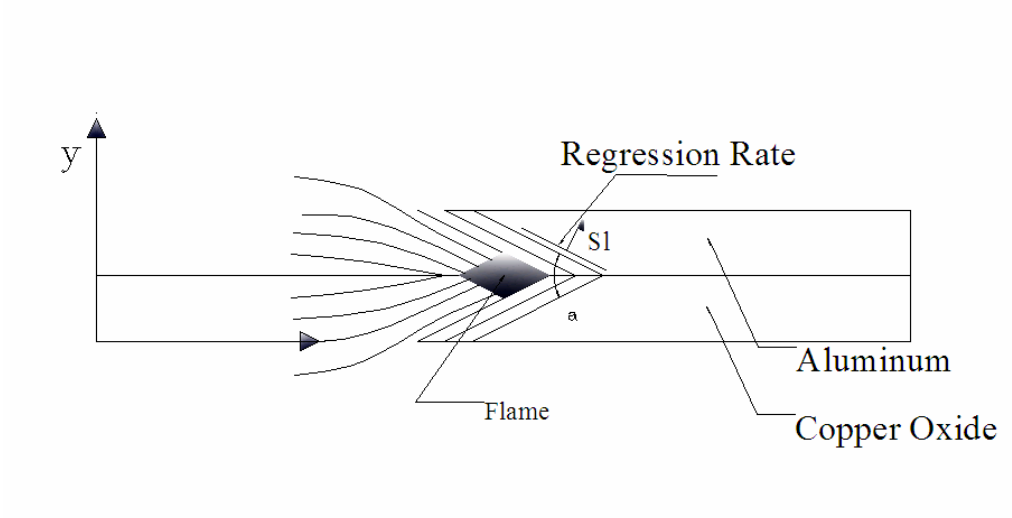

Figure 4-2 : Typical Axi-symmetric Flame

In the idealized set up in Figure 4.2, the control volume moves through the stationary material within the sample frame. The thin reaction zone (black box) is commonly referred to as

flame, has two separate sections, cool and hot zone (figure 4.3). Front part of the flame is the cool zone and the area behind with the hot products is the hot zone. As the flame moves along the direction of flame propagation, the temperature and pressure rise in the unburned material.

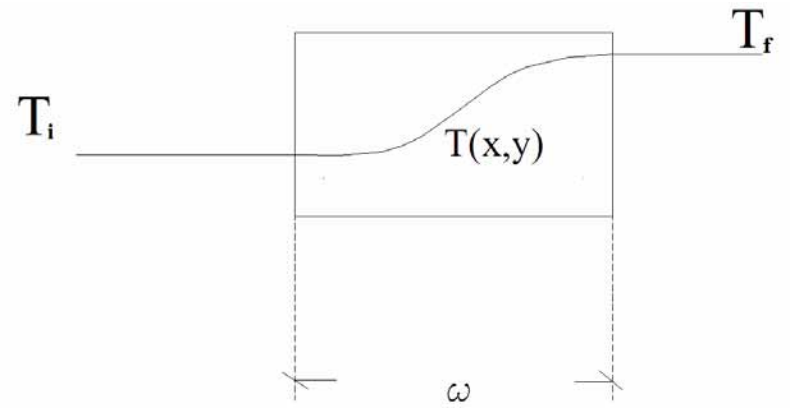

Figure 4-3 : Steady State Temperature profile within flame

The primary objective of the numerical solution is to first develop a simple governing equation expressing the conservation of mass, species, and energy for the control volume. Our approach is to define the physical characteristics of the flame such as speed and temperature, and then establish the governing equations (Appendix B) related to the control volume (black box). Solution of the governing equation for a specific control volume will require the speed and length of the flame.

Substrate materials can control the reaction front by the heat sink. A number of materials with different thicknesses have been tested as substrate for standard thin film. The theory of moving the heat source over the solid [40-50] was used to show the distribution of the temperature over substrate. At this stage, linear heat sources were used as a simple flame front over a single substrate. Experiments show highly conductive materials in substrate can quench the flame.

To define a model that shows the relationship between the heat front and speed of propagation, composite substrates were used. This substrate thickness was varied systematically to vary the heat absorption. Subsequently, the temperature profiles can be obtained from the numerical solution over composite substrate. The maximum temperature on the flame is controlled by the speed of propagation and the height of the substrate.

Conservation of energy principle can be utilized to establish the relationship between temperature profile and speed of propagation. Conservation of mass principle can be utilized to establish the relationship between conservation of species within the reaction and speed of propagation. Temperature is related to the speed of propagation. The control volume moves with the flame front so that the concentration profile need not be considered.

Laminar Flame

Several theories of laminar flames have been proposed for decades and several simplifying assumptions made by [51,52]. In this paper, a simple axisymmetric case is considered for a laminar flame. Figure 4.2 shows the typical axisymmetric flame, which is propagated in the sample. Existing similar media on both sides of the reaction zone satisfies this assumption. Depositing in a thin layer of the material in nanoscale is similar to premixing of the material. Although solving governing equation in premixed case is easier than the un-premixed case, the specific dimension for each individual reactant in governing equations is neglected.

Physical Description

The essential characteristics of the laminar premixed flame are qualitatively described and simplified analysis of flames is developed. This will allow us to observe the influencing factors

related to the laminar flame speed and thickness. Flame is self-sustaining propagation of localized combustion zone at subsonic velocity. In addition, it is possible for combustion to propagate at speed of sound within material and such a wave is called detonation. Temperature profile throughout the flame is the most important characteristic of the flame. Two dimensional temperature profile is dependent on the overall reaction. Regression rate, $S_{L,}$ (Figure 4.4) is the speed of unburned mixture in a free propagating combustion approaching the flame perpendicular to the control volume at a fixed reference. The fixed reference frame is a stationary frame relative to a laboratory reference frame. Regression rate, S_L, can be divided into the speed of the flame in X and Y directions.

In a two dimensional study, control volume sweeps through the reaction path (x-axis) in a conical profile with a specific radius (r).

$$v_x = S_L.\cos\left(\frac{\alpha}{2}\right) \tag{4.1}$$

$$v_r = S_L.Sin\left(\frac{\alpha}{2}\right) \tag{4.2}$$

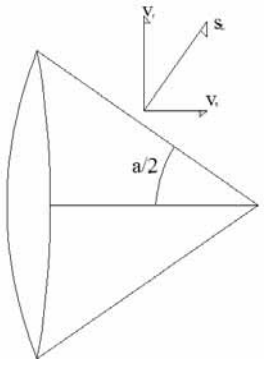

Figure 4-4 : Axisymmetric Velocity of the Flame

Two Dimensional Temperature Distributions on Single Substrate

Based on the theory of moving heat source, heat can penetrate inside the substrate in all directions. For a moving point heat source, general equation of heat transfer based on Fourier's law is:

$$\frac{d^2T}{dx^2}+\frac{d^2T}{dy^2}+\frac{d^2T}{dz^2}=\left(\frac{1}{\alpha}\right)\frac{dT}{dt} \tag{4.3}$$

Neglecting the z-dimension temperature variation, the two-dimensional equation is

$$\frac{d^2T}{dx^2}+\frac{d^2T}{dy^2}=\left(\frac{1}{\alpha}\right)\frac{dT}{dt} \tag{4.4}$$

Assuming constant speed of propagation and using the chain rule,

$$\frac{dT}{dt}=\frac{dT}{dx}\cdot\frac{dx}{dt}+\frac{dT}{dy}\cdot\frac{dy}{dt} \tag{4.5}$$

$$\frac{dx}{dt}=v_x \text{ and} \qquad \frac{dy}{dt}=v_y=0 \qquad \frac{dT}{dt}=\frac{dT}{dx}\cdot v_x \tag{4.6}$$

Then, the governing equation is simplified to:

$$\frac{d^2T}{dx^2}+\frac{d^2T}{dy^2}=\left(\frac{v_x}{\alpha}\right)\frac{dT}{dx} \tag{4.7}$$

Based on the flame configuration given in figure 4.5 the temperature distribution for the moving point source is:

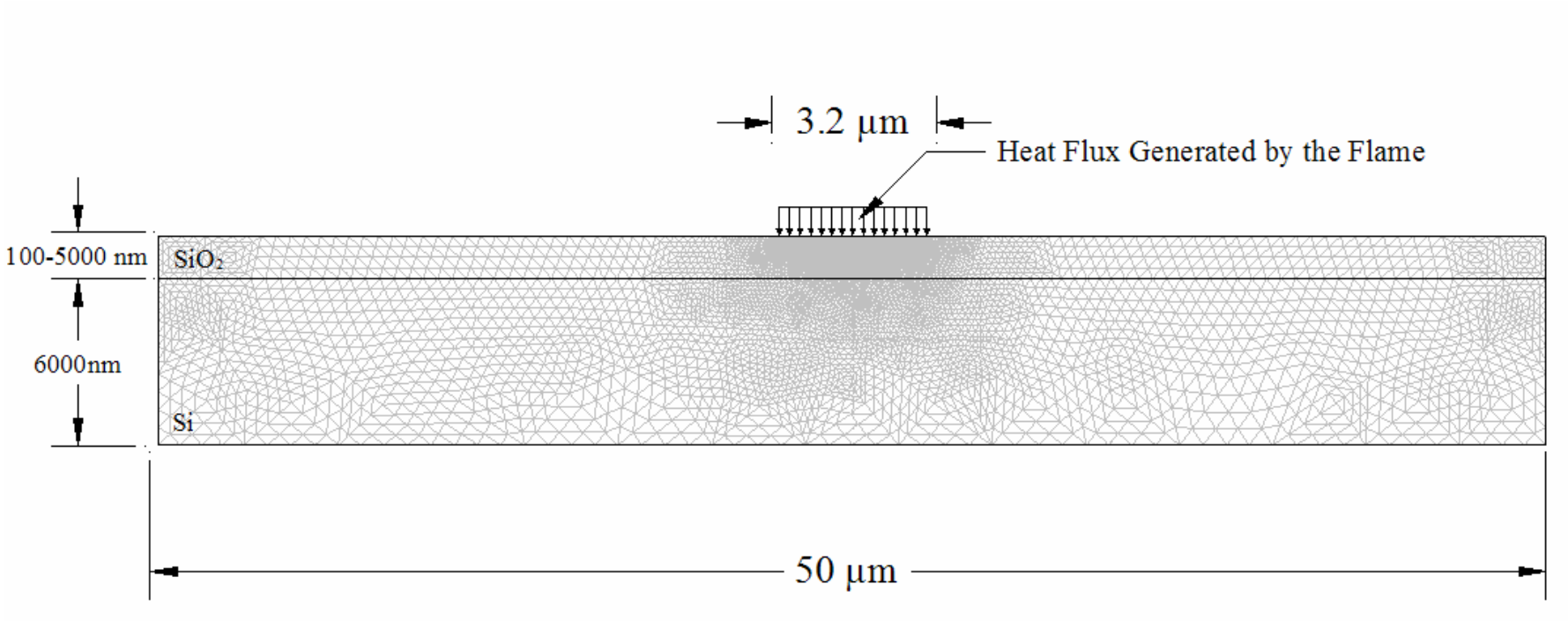

Figure 4-5 : Computational Dom

$$\frac{\partial T}{\partial x}(x = \pm\infty, y) = 0$$

$$k\frac{\partial T}{\partial y}(x = \pm \omega/2, y = 0) = q$$

$$\frac{\partial T}{\partial y}(-\infty \le x \le -\omega/2, y = 0) = 0$$

$$\frac{\partial T}{\partial y}(\omega/2 \le x \le +\infty, y = 0) = 0$$

$$\frac{\partial T}{\partial y}(x, y = \infty) = 0 \tag{4.8}$$

Closed Form Solution

The moving heat source problem over a single substrate was initially solved by Carslaw and Jaeger [50, 53]. Rosenthal [54] developed the theory of the heat motion and provided the closed form solution for the linear two-dimensional heat source. Moving heat source was modeled for a number of applications such as laser machining [55, 56], and friction stir welding [57]. In this study, a similar approach was used to relate the speed of flame, v_x, and heat flux, which is generated inside the flame with temperature distribution on the substrate. Closed form solution for a single moving source for eq. (4.7) for a single infinite substrate is:

$$T - T_i = \left(\frac{q}{2\pi k}\right) K_0\left(\frac{v_x r}{2\alpha}\right) \exp(-v_x x / 2\alpha) \tag{4.9}$$

where K_0 is the Bessel function of the second kind and q, α, and k are heat flux, thermal diffusivity and conductivity respectively.

For a two-dimensional heat source, Weichert and Schonert [55] extended the closed form solution given in eq. (4.9) inside a single slab. They used the coordinate transformation to solve the one-dimensional heat source with the length of ω in the direction of the motion as shown in figure 4.5. The solution for a two-dimensional moving linear heat source of width, ω, is given by

$$T - T_i = \left(\frac{q}{2\pi k}\right) \int_{-\omega/2}^{+\omega/2} K_0\left(\frac{v_x r}{2\alpha}\right) \exp(-v_x \xi / 2\alpha) d\xi \ . \tag{4.10}$$

Although using a single substrate shows the critical role played by heat front propagation and speed of reaction, it is not capable of controlling the heat front. However, closed form solutions to layered substrates are not possible. It is to be noted that whether an analytical solution or a numerical solution is sought, the speed of propagation of the flame front needs to be known. Secondly, the solution given in eq. (4.10) is for a single substrate. Therefore, eq. (4.7) needs to be solved numerically for a flame front on a SiO_2-Si substrate. Before solving this equation with the boundary condition in eq. (4.8), speed of flame propagation needs to be measured. This speed, v_x, will be used as a constant in the numerical solution procedure.

Experimental Procedure

In order to measure some of the major characteristics of the flame, reaction variables should be defined and controlled. Heat generation inside of the control volume plays a main role for the self-propagation of the reaction. Experimentally, it is possible to control the amount of heat during the reaction by creating a variable heat sink as substrate for the thin film. In order to

measure some of the characteristics of the flame, long strips of the multilayer thin film were deposited on the substrate.

Measurement Techniques for Speed of Flame

Tappan [58] used different types of thin film geometry to create a controllable environment to measure the characteristics of the flame in microscale. Controlling some of the characteristics such as speed and length of the flame are necessary to create a controlled environment. Rossi [59] used different types of thin film geometry to create controllable environment. This environment is used in many micro thin film materials in mechanical and electrical devices.

Layered Al/CuO MIC having a total thickness of 3.2 μm was prepared by magnetron sputter deposition. An Al layer thickness of 26 nm and CuO layer thickness of 54 nm were used to provide a bi-layer period of 80 nm for a standard sample configuration, as illustrated in Figure 4.6.

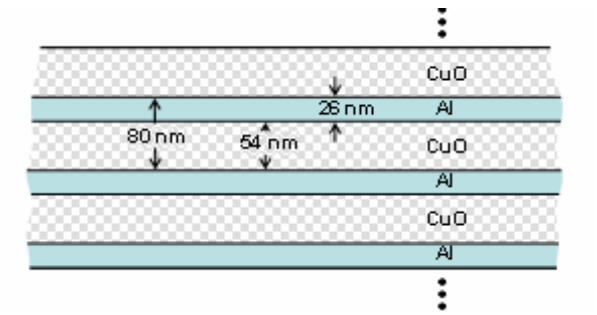

Figure 4-6 : Multilayer Al and CuO (MIC)

An electronic time-of-flight technique was developed using patterned strips of layered MIC on a substrate (Figure 4.6), wherein the passage of the reaction front passes copper contacts spaced along the length of the strip (Figure 4.7). As the flame ignites on one side of the thin filmstrip, it can propagate with constant speed across the sample. The flame can burn each

copper strip in equal time increments. This configuration produced a stepwise change voltage, which was digitally acquired and analyzed to determine the propagation velocity. Each copper probe is connected to a series of resistances in the circuit; Figure (4.7) shows a typical circuit that was used in this experiment. Voltage output can drop at the instant that flame passes across copper probes. This stepwise change in reduced voltage is shown in figure 4.8.

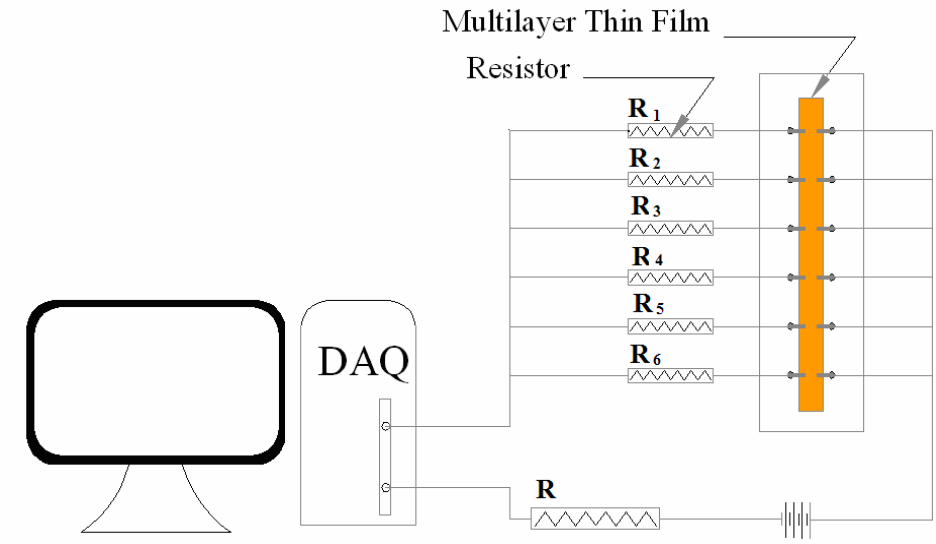

R	5000Ω
R1	4300Ω
R2	6100Ω
R3	5000Ω
R4	3000Ω
R5	2000Ω
R6	1000Ω

Figure 4-7 : Configuration Set up for High Speed Measurement

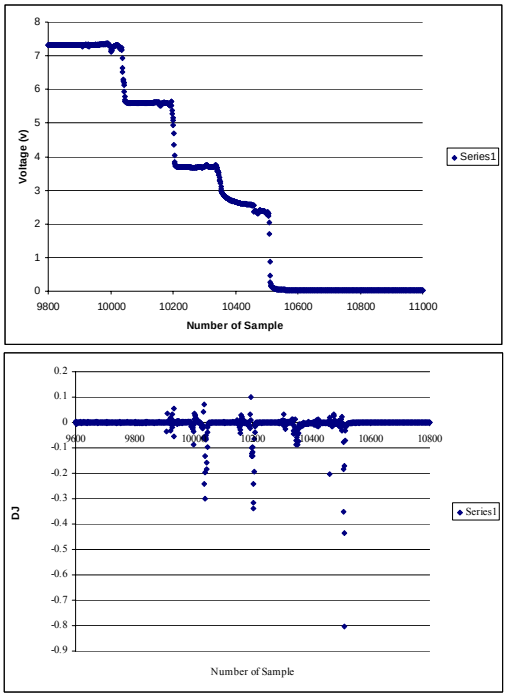

Figure 4-8 : a) Example of electronic time of –flight measurement of reaction velocity for layered Al/CuO MIC deposited on a substrate; b) Voltage gradient to obtain accurate measurement of distance.

This technique gives a much higher accuracy than spectroscopy measurement. The camera, which is used in the spectroscopy techniques, is capable of capturing 60,000 frames per second. Typically, the time of –flight technique provides an uncertainty of 50 μs for a speed of propagation of 50 m/s. Table (4.1) shows a typical experiment result for time of voltage drops in three equal part of the sample. By comparing the voltage gradient at the lead and lag part of the drop, the velocities were computed. This dual computation shows that there is adequate confidence in the velocity measurement.

Table 4-1 : Typical Speed of Flame in Lead and Lag Cases

Lead (Top)	Number of Sample	Time (s)	Speed m/s	Average Speed
10035				
10194	159	0.00019875	50.31	
10344	150	0.0001875	53.33	
10502	158	0.0001975	50.63	51.42
Lag (Bottom)				
10038				
10203	165	0.00020625	48.48	
10353	150	0.0001875	53.33	
10510	157	0.00019625	50.95	50.92

Effect of Single Substrate

It is possible to control the heat at the front of the flame by placing a substrate underneath the heat source. Absorbing the heat that is generated in the flame can reduce the speed of the flame and quench the reaction. The substrate can absorb a significant amount of the heat at the front of the flame. Using different materials with high to low thermal conductivity can reduce the speed of the flame or even stop it. Poorly conductive materials absorb less heat, can boost the speed of the flame, and can cause reactions at a higher rate. On the other hand, highly conductive materials have opposite effects on the speed of the flame. Some experiments with highly conductive materials in the substrates show reactions only on a few top layers of the thin film and heat does not penetrate to the bottom layers of the thin film.

Several types of substrates for MIC thin films were examined. Single substrate samples were prepared on glass and kapton (Table 4.2). For the typical structure having an 80 nm bilayer period and a total thickness of 3.2 μm, burn rates in the range of 14 m/s for kapton and 45m/s for glass were observed. Composite substrates were prepared on Si wafer having a thin layer of

photoresist or SiO_2. The thermal conductivity of each material can impact the effectiveness of the heat front. For example, kapton is more conductive than photoresist or glass, consequently the speed of reaction significantly drop

Table 4-2 : Speed of Flame on Single and Composite Substrates

Substrate	Thermal conductivity (W/m.k)	Thickness (μm)	Sample rate (kHz)	Speed of reaction (m/s)	Average Speed (m/s)
glass	1.4	1000	800, 1000	45.61, 44.78, 51, 44.76, 47.17	46.75
photo resist/Si	0.2	1.1	800	52.94, 54.97	53.955
photo resist/Si	0.2	10	800, 1000	61.05, 61.86,	61.45
photo resist/Si	0.2	2	800	17.20, quench	quenched
SiO2/Si	1.4	0.03	1000	quench	quenched
SiO2/Si	1.4	0.1	1000	quench	quenched
SiO2/Si	1.4	0.2	1000	quench	quenched
SiO2/Si	1.4	0.5	1000	41.66, 43.52, 42.97	42.72
SiO2/Si	1.4	2	1000	43.1,42.73, 41.78	42.54

Heat loss to the substrate heat during the reaction has a main role to play in the determination of the speed of the flame. The heat can become a controlled variable by utilizing different heat sinks for the flame. A material with high conductivity can quench the reaction completely. By depositing a thin layer of material with low conductivity such as silica or photoresist, a part of the generated heat can be absorbed by the substrate. Thickness of deposition can be a variable and will affect the speed of the flame.

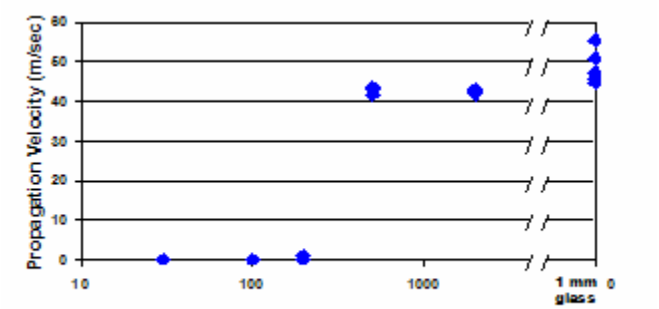

Figure 4-9 : MIC Speed of flame (burn rate) as Function of Thermal Insulation Thickness of SiO_2

Similar velocities to a single substrate were observed for this structure on Si substrates having a thick intervening layer of SiO_2 to provide thermal insulation. When this structure was prepared adhered to a Si substrate without a thermal insulation layer, no self-propagating reaction was observed, i.e., the reaction was effectively quenched (Table 4.2). Figure 4.9 also shows that the average speed or quenching depends on the thickness of SiO_2 substrate as well as the conductivity. The dependence of the reaction velocity on the substrate is an example of how the reaction process may be inferred by the measurement of reaction velocity for a series of samples. Thermal penetration depth, δ, of the moving reaction front into the thermally grown SiO_2 surface layer is estimated by varying the thickness, hSiO2, of the layer. Figure 4.9 shows that the reaction is completely quenched for SiO_2 layer of less than 200 nm. The speed of the flame propagation seems to be more or less a constant at 40 m/s for SiO_2 Layers of 1 μm and 2 μm. For a 10 μm photoresist layer the speed is respectively 60 m/s, however at 2 μm thickness the reaction is quenched.

For the case of hSiO2 > δ, the reaction velocity is expected to be similar to that of the bulk glass substrate. For hSiO2 < δ, a reduced reaction velocity is expected due to the increased loss of the heat of the reaction into the higher thermal conductivity silicon. The sudden decrease in

velocity for hSiO2 less than 500 nm in figure 4.9 indicates this to be an upper bound for the thermal penetration depth, δ. If we use this distance and the thermal diffusivity of SiO_2, α, in the simple approximation, $\delta = \sqrt{4\alpha t}$, we get an estimate of the time, t, that the composite substrate is exposed to the moving reaction front as t = 69 ns. The measured velocity of the reaction front, vx = 43 m/s, allows us to calculate its effective width, w, as 3 μm.

Numerical Procedure

The main objective of this portion of the experiment is the numerical solution of two-dimensional heat conduction in a linear moving heat. Heat moves along the X direction and travels with constant speed of v_x over a composite substrate Figure 4.5. This two dimensional conduction model can not be solved analytically; therefore, numerical solutions are sought to determine the temperature profile. One of the ways to validate solutions is to solve the extreme case of the composite substrate and compare it to the analytical solution in moving source over a single substrate, given by eq. (4.10). In this case, a finite element method and explicit technique was used to develop a computer code to compare the result in a commercial code, Comsol.

Governing Equation and Boundary Conditions

The governing equation for the linear moving heat, which is stretched along the x direction and moves in the same direction with constant speed of v_x over composite substrate given in figure 4.5 are:

$$\frac{\partial^2 T}{\partial x^2} + \frac{\partial^2 T}{\partial y^2} = \frac{v}{\alpha_1}\frac{\partial T}{\partial x} \tag{4.11}$$

$$\frac{\partial^2 T}{\partial x^2} + \frac{\partial^2 T}{\partial y^2} = \frac{v}{\alpha_2}\frac{\partial T}{\partial x} \tag{4.12}$$

In this case, α_1 and α_2 are α_{SiO_2} and α_{Si} respectively, which are the thermal diffusion coefficient for silica and silicon relatively. Boundary conditions are similar for a single substrate:

$$\frac{\partial T}{\partial x}(x = -\infty, y) = 0$$

$$T(x = +\infty, y) = 300K$$

$$k\frac{\partial T}{\partial y}(x = \pm \omega/2, y = 0) = q$$

$$\frac{\partial T}{\partial y}(-\infty \le x \le -\omega/2\, 0, y = 0) = 0$$

$$\frac{\partial T}{\partial y}(\omega/2 \le x \le +\infty, y = 0) = 0$$

$$T(x, y = \infty) = 300\,\mathrm{K} \tag{4.8}$$

Appropriate space discretization can improve the accuracy and stability of the solutions. Variable mesh was used for this problem. Number of elements were increased along the interface and heat source.

Explicit Method

Explicit method was used to carry out the computations. Since the flame speed is constant, time is proportional to x direction of motion. Therefore forward differencing was used for x direction and central differencing was used for y direction.

$$\frac{\partial T}{\partial x} = \frac{T_{i+1} - T_i}{\Delta x} + O(\Delta x) \qquad \text{(Forward differencing)} \tag{4.13}$$

$$\frac{\partial^2 T}{\partial y^2} = \frac{T_{i+1} - T_i + T_{i-1}}{\Delta y^2} + O(\Delta y^2) \quad \text{(Central differencing)} \tag{4.14}$$

$$\frac{\partial^2 T}{\partial x^2} = \frac{T_{i+2} + T_i - 2T_{i+1}}{\Delta x^2} + O(\Delta x^2) \quad \text{(Forward differencing)} \tag{4.15}$$

The finite difference form of the differential equation is

$$\frac{v}{\alpha}\left(\frac{T_{i+1} - T_i}{\Delta x}\right) = \frac{T_{i+1} - T_i + T_{i-1}}{\Delta y^2} + \frac{T_{i+2} + T_i - 2T_{i+1}}{\Delta x^2} + O(\Delta y^2, \Delta x) \tag{4.16}$$

At the interface between silica and silicon, Pletcher [60] recommends a harmonic mean thermal conductivity, k_e, as the numerical value of heat conductivity at the interface of two materials.

$$k_e = \frac{2k_{SiO_2} \cdot k_{Si}}{k_{SiO_2} + k_{Si}} \tag{4.17}$$

k_{SiO_2} and k_{Si} is the thermal conductivity of silica and silicon.

$$\frac{v}{\alpha_{SiO_2}}\left(\frac{T_{i+1} - T_i}{\Delta x}\right) = \frac{T_{i+1} - T_i + T_{i-1}}{\Delta y^2} + \frac{T_{i+2} + T_i - 2T_{i+1}}{\Delta x^2} \tag{4.18}$$

$$\frac{v}{\alpha_{Si}}\left(\frac{T_{i+1} - T_i}{\Delta x}\right) = \frac{T_{i+1} - T_i + T_{i-1}}{\Delta y^2} + \frac{T_{i+2} + T_i - 2T_{i+1}}{\Delta x^2} \tag{4.19}$$

$$\frac{v}{\alpha_e}\left(\frac{T_{i+1} - T_i}{\Delta x}\right) = \frac{T_{i+1} - T_i + T_{i-1}}{\Delta y^2} + \frac{T_{i+2} + T_i - 2T_{i+1}}{\Delta x^2} \tag{4.20}$$

α_e is the thermal diffusion coefficient based on harmonic mean, k_e, for the elements at the interface of silica and silicon.

Equation (4.18), (4.19) and (4.20) were solved simultaneously using an iteration technique to obtain the temperature profiles. To reduce the uncertainty and increase the accuracy of numerical

solutions, geometry of substrate is modified. Heat flux on each side of the substrate should approach to zero.

To find the appropriate number of elements in the computational domain, random number of elements were picked and the maximum temperature in exact same geometry were compared. Figure (4.10) shows solution is getting more accurate by increasing the number of elements in same geometry due to limitation on processing. 175000-200000 elements range was chosen for these calculations. In fact, the uncertainty is controlled by $\pm 0.5\,\%$.

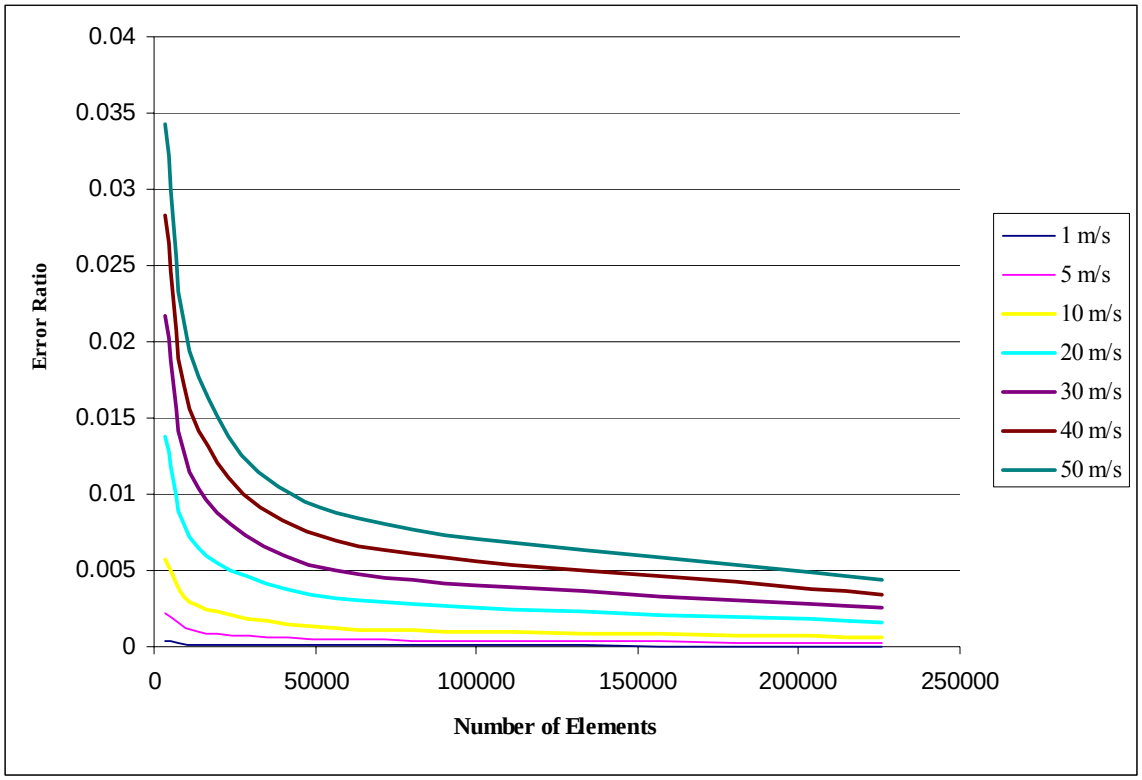

Figure 4-10 : Relative Error with respect to the number of elements

Now with the velocity measurement, equation (4.7) with the boundary condition (4.8) can be solved. Composite substrates can demonstrate practical ways to compare and link characteristics

of the flame, such as length of the flame, speed of propagation, conductive heat flux and temperature destruction in different situations. The energetic thin film heat generation is constant and no heat is lost on the top of the heat source through either convection or radiation. Physical properties of the substrate in each case are known for different cases. Furthermore, speed of the flame has been measured for each case based on the time-of -flight technique.

Numerical approach was used to model the moving heat source with width, ω, on the composite substrate. Control volume approach was used to balance the heat flux at the interface in each unit cell. Heat flows from the heat source through the SiO_2 and the interface, dissipating to the silicon substrate.

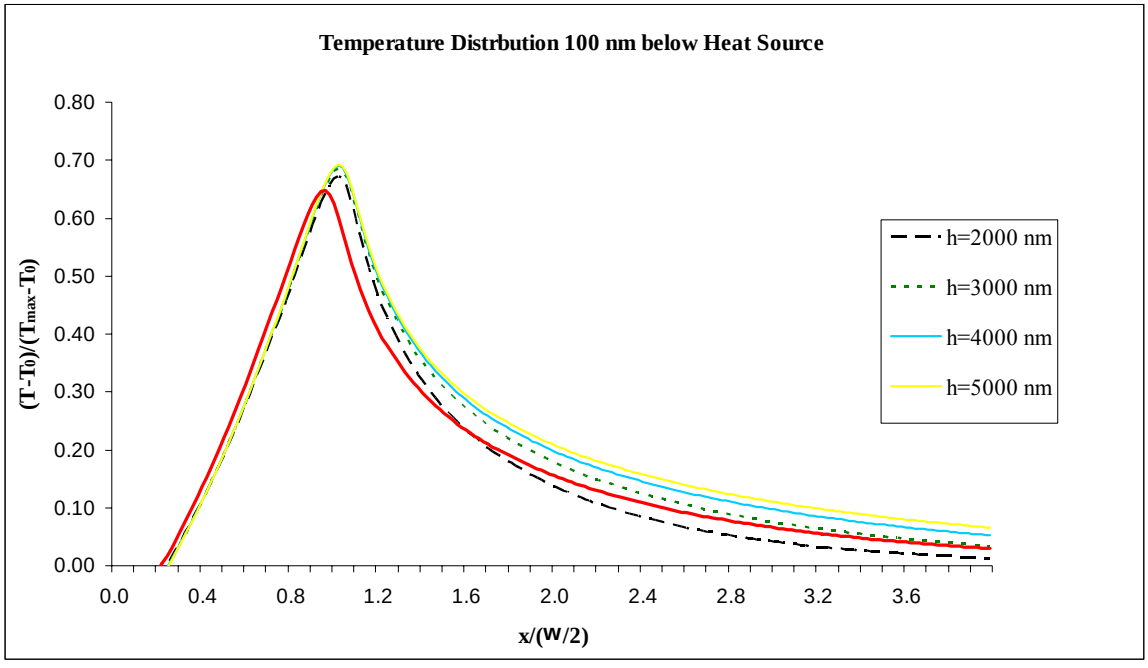

Figure 4-11.: Temperature distribution 100 nm below the heat source. Ω for this case was taken to be 3 μm h is the SiO_2 substrate thickness

In figure 4.11, non-dimensional profiles of temperature 100 nm below the heat source are given for different SiO_2 substrate thickness, h. The maximum temperature for all cases is at the

leading edge of the heat source. As the substrate thickness increases, the temperature profile become self-similar for h>1000nm and compare well with the analytical solution given in the eq. (4.10). As h increases, the peak temperature increases. In addition, for lower thicknesses, temperature reaches ambient temperature earlier in the direction of propagation.

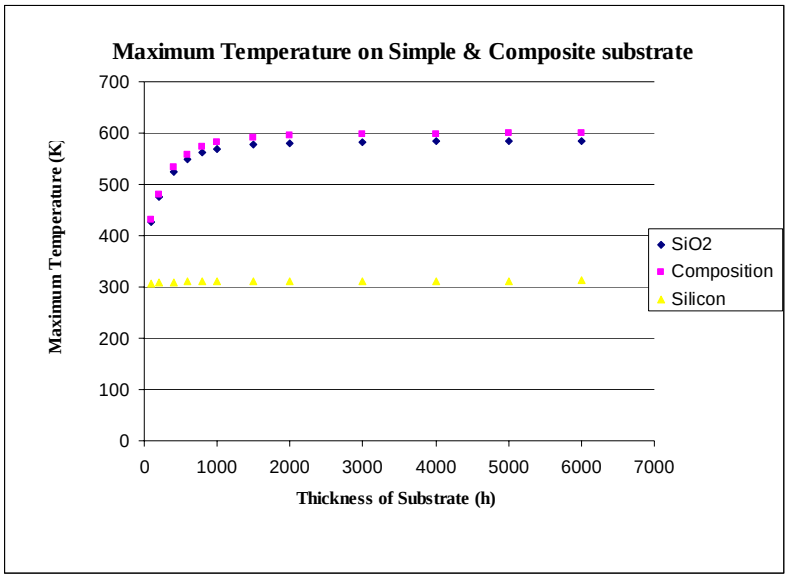

Figure 4-12 : Maximum temperature distributed on simple and composite Substrates for various thicknesses

Figure 4.12 shows the variation of maximum temperature with substrate thickness. There appears to be very little difference between a single substrate of Silica and a composite Si-SiO_2 substrate. This shows the effectiveness of the composite substrate. As the substrate thickness increases the maximum temperature increases until about 1μm. Beyond 1μm, the maximum temperature becomes constant for both single and composite substrates.

Summary

This chapter deals with the reaction of dense Metastable Intermolecular Composition (MIC). Energy density of MIC nanofilms is much higher than conventional films. The problem of a multilayer thin film of Aluminum and Copper oxide has been solved with varying substrate material and thicknesses. In order to solve this conduction problem, speed of propagation was experimentally determined using a time of–flight technique. The experiment shows that the reaction is completely quenched for the silicon layer of less than 200 nm. The speed of reaction seems to be constant at 40 m/s for silica layers over 1 μm. Different substrate material such as glass, kapton, and photoresist were used.

The numerical solution shows the temperature profiles become self similar for substrate thickness beyond 1 μm. Beyond 1 μm, the maximum temperature stays constant for both single and composite substrates, showing the effectiveness of composite substrates both experimentally and numerically.

CHAPTER 5
SUMMARY

Significant progress has been made in understanding the reaction of the dense Metastable Intermolecular Composition (MIC). This problem has been solved in 3 steps that are tied together, yet increasing in complexity. For the MIC layer, Aluminum and Copper oxide have been considered since there are available data in the literature. The goal is to increase the energy density of MIC compared to conventional materials and analyze the speed of reaction for various substrates.

However, this is a formidable problem to include the combustion phenomena and obtain analytical results. Therefore, as a first step, a one-dimensional model was developed for 20 pairs of a multi-layer of aluminum and copper oxide. This problem was solved using an assumed value of constant atomic diffusion in Arrhenius' equation to obtain the velocity of self-propagation. Using the maximum and minimum measured velocities in a similar configuration, the activation energy was computed and was found to be significantly different. One of the setbacks is that multiple values of activation energy can be obtained using this model. Another weakness is that the speed of propagation is independent of the individual thicknesses of CuO and Al. Experimental data does not support this theory in the Al/CuO reaction. Thus, while it is possible to solve multiple MIC layers in the direction of propagation of reaction, the model ignores diffusion in the lateral direction and therefore, it is difficult to validate this model with experimental data.

MIC reaction creates an enormous amount of energy, which causes phase transformation throughout the reaction. For the purpose of theoretical calculations, as a second step in this thesis, the scope and size of the process was limited to an adiabatic unit cell of a single layer of aluminum and copper oxide in an ideal reaction was considered. The physical surface area in this study is limited to a cross section of a rectangular prism. Total amount of heat and final temperature of unit cell are calculated based on conservation of mass and energy. Temperature profiles based on heat generation and phase transformation of reactants have been calculated. While aluminum and copper oxide are being consumed, they are transformed from solid to liquid. The process generates copper and alumina in solid, liquid, and gas phases. Numerical solution shows that 2793±100K is the highest possible temperature for the reaction. This model confirmed the highest possible temperature during reaction of 2920^{o}C ± 5% obtained in the literature; however, this model was unable to provide the important flame characteristics.

As a third step in the thesis, a two-dimensional model was developed introducing the flame at the interface. A black box theory was used so that the problem can be simplified to a moving line source conduction problem. Controllable environment was created for the multilayer thin film of aluminum and copper oxide to eliminate the number of effective variables that affect the speed of propagation. Transformable heat of reaction was used to control the speed of propagation. Varying the thickness of silica on top a silicon substrate controlled the speed of propagation. In order to solve this conduction problem, speed of propagation was experimentally determined using a time-of–flight technique. It was determined from the experiment that the reaction is completely quenched for the silicon layer of less than 200 nm. The speed of reaction seems to be

constant at 40 m/s for silica layers over 1 μm. Different substrate material such as glass, kapton, and photoresist were used.

The numerical solution shows the temperature profiles become self similar for substrate thickness beyond 1 μm. Beyond 1 μm, the maximum temperature stays constant for both single and composite substrates, showing the effectiveness of composite substrates both experimentally and numerically.

Future Work

The two-dimensional problem can be extended to three-dimensions and also to include thermal transport and atomic diffusion. Black box model can be improved in many different ways. The physical source can be defined based on chemical reaction and combined in the current moving heat source model. Exact volumetric heat generation can be applied to the flame box, and the length of flame defined and measured numerically. Flame characteristics can only be captured by complex models that take into account reaction kinetics and a number of physical variables, and these need to be incorporated into realistic and mechanistic future models.

APPENDIX A
PROPERTIES OF THE MATERIALS

Table A-1 : Physical Properties of Reactants and Product

	Density (g/cm3)	Melting point (K)	Latent heat (cal/g)	Boiling point (K)	Latent heat of vaporization (cal/g)	C_p (J/ kg .k)
Al	**2.702**	**933**	**94.8**	**2723**	**2720**	**903**
Cu	**8.933**	**1356**	**32**	**2793**	**1210**	**385**
CuO	**6.310**	**1358**	**35.4**			**[14]**
Cu_2O	**6.000**	**1503**	**93.6**	**2073**		**[14]**
Al_2O_3	**3.965**	**2325**	**250.6**	**3273**	**1130**	**[14]**

APPENDIX B
GOVERNING EQUATIONS

Governing Equation

To define flame propagation, conservation of mass, species and energy are applied in the two dimensional control volume.

Mass Conservation

The general form for mass conservation is defined as:

$$\frac{\partial \rho}{\partial t} + \nabla \cdot (\rho \cdot v) = 0 \qquad \text{(B.1)}$$

$\frac{\partial \rho}{\partial t}$ is rate of gain of the mass per unit volume

$\nabla \cdot (\rho \cdot v)$ is net rate of mass flow out per unit volume

For steady flow,

$$\nabla \cdot (\rho \cdot v) = 0 \qquad \text{(B.2)}$$

For the axisymmetric system, equation (53) is expanded to

$$\frac{1}{r}\frac{\partial}{\partial r}\left(r.\rho.v_r\right) + \frac{\partial}{\partial x}\left(\rho.v_x\right) = 0 \qquad \text{(B.3)}$$

Species Conservation

The general form for mass conservation of species is expressed as

$$\frac{\partial \rho.Y_i}{\partial t} + \nabla.m_i'' = m_i''' \qquad \text{(B.4)}$$

$\frac{\partial \rho.Y_i}{\partial t}$ is the rate of gain of mass of species i per unit volume

$\nabla.m_i''$ is net rate of mass flow of the species i out by diffusion and bulk flow per unit volume

m_i''' is net rate of mass production of species per unit volume

The mass flux of i, m_i is defined by the mass average velocity i, v_i as follows:

$$m_i'' \equiv \rho . Y_i . v_i \tag{B.5}$$

The sum of all of the individual species mass flux is the mixture mass flux.

$$\sum m_i'' = \sum \left(\rho . Y_i . v_i \right) = m'' \qquad\qquad m'' \equiv \rho . V \tag{B.7), (B.6}$$

The mass average velocity V is:

$$V = \sum \left(Y_i v_i \right) \tag{B.8}$$

This (V) is the velocity known as bulk velocity. The difference between the spices and bulk velocity is defined as diffusional velocity.

$v_{i,diff} \equiv v_i - V$ The diffusion mass flux can be expressed in term of diffusion velocity.

$$m''_{i,diff} \equiv \rho . Y_i \left(v_i - V \right) = \rho . Y_i v_{i,diff} \tag{B.9}$$

The total species mass flux is the sum of the bulk flow and diffusion contribution.

$$m_{i^i}'' = m'' Y_i + m''_{i,diff} \tag{B.10}$$

$$\rho . Y_I v_i = \rho . Y_i V + \rho . Y_i v_{i,diff} \tag{B.11}$$

Rewriting the general species conservation equation based on mass diffusion:

$$\frac{\partial \rho . Y_i}{\partial t} + \nabla . \left[\rho . Y_i \left(V + v_{i,diff} \right) \right] = m_i''' \tag{B.12}$$

For the axisymmetric geometry the corresponding conservation for the binary mixture is:

$$\frac{1}{r}\frac{\partial}{\partial r}\left(r . \rho . v_r Y_A \right) + \frac{1}{r}\frac{\partial}{\partial x}\left(r . \rho . v_x . Y_A \right) - \frac{1}{r}\frac{\partial}{\partial r}\left(r . \rho . D \frac{\partial Y_A}{\partial r} \right) = -m_A'' \tag{B.13}$$

Y is the mass fraction

m is the mass

m’ is mass flow rate

m” is the mass flux

m”’ is mass production rate per unit volume

Energy Conservation

Conservation of energy for laminar premixed flame is simplified by Shvab-Zeldovich [61]. Shvab-Zeldovich energy equation shows total difference between the rate of enthalpy transport by convection and diffusion is equal to the rate of enthalpy production by chemical reaction.

$$\nabla.\left[m''\int c_p dT - \rho.D\nabla\left(\int c_p dT\right)\right] = -\sum\left(h^0{}_f .m_i'''\right) \tag{B.14}$$

For the two-dimensional axisymmetric case, the equation is expanded to

$$\frac{1}{r}\frac{\partial}{\partial x}\left(r.\rho.v_x\int c_p dT\right)+\frac{1}{r}\frac{\partial}{\partial r}\left(r.\rho.v_r\int c_p dT\right)-\frac{1}{r}\frac{\partial}{\partial r}\left(r.\rho.D\frac{\partial}{\partial r}\int c_p dT\right) = -\sum h^0{}_f .m''_i \tag{B.15}$$

Mass flux can be derived based on the speed of flame

$$m'' = \rho_u .S_L \tag{B.16}$$

Length of the flame can be calculated based on 95-99% of the final temperature

$$T(\delta) = 95\%T_f \tag{B.17}$$

REFERENCES

1) Blobaum K. J., A. J. Wagner, J. M. Plitzko, D. Van Heerden, and T. P. Weihs: Investigating the reaction path and growth kinetics in CuO_x /Al multilayer foils, J. Appl. Phys., Vol. **94**, 2003.

2) Miziolek, A. W: Nanoenergetics: An Emerging Technology Area of National Importance, AMPTIAC Quarterly, Vol. **6**, #1, pp. 43-48, 2002.

3) Clevenger, L. A., Thompson, C. V., and Tu, K. N: Explosive silicidation in nickel/amorphous-silicon multilayer thin films, Journal of Applied Physics, Vol. **67**, # 6, pp. 2894-2898. 1990.

4) Ma, E., Thompson, C. V., Clevenger, L. A., and Tu, K. N: Self-propagating explosive reactions in Al/Ni multilayer thin films, Applied Physics Letters, Vol **57**, number 12, pp. 1262-1264. 1990.

5) Gavens, A. J., Van Heerden, D., Mann, A. B., Reiss, M. E., and Weihs, T. P: Effect of intermixing on self-propagating exothermic reactions in Al/Ni nano-laminate foils, Journal of Applied Physics, Vol **87** #3, pp.1255-1263, 2000.

6) Besnoin, E., Cerutti, S., Knio, O. M., and Weihs, T. P: Effect of reactant and product melting on self-propagating reactions in multilayer foils, Journal of Applied Physics, Vol. **92**, #9, pp.5474-5481, 2002.

7) Blobaum, K. J., Reiss, M. E., Plitzko Lawrence, J. M., and Weihs, T. P: Deposition and characterization of a self-propagating CuO_x/Al thermite reaction in a multilayer foil geometry, Journal of Applied Physics, Vol.**94**, #5, pp.2915-2922. 2003.

8) Rogachev, A. S., A. S., Grigoryan, H. E., Illarionova, Kanel, I. G., Merzhanov, A. E., Nosyrev, A. N., Sachkova, N. V., Khvesyuk, V. I., and Tsygankov, P. A: gasless Combustion of Ti-Al Bimetallic Multilayer nanofoils, Combustion, Explosion, and Shock Waves, Vol**40**, number 2, pages 166-171, 2004.

9) Gachon, J.-C., Rogachev, A. S., Grigoryan, H. E., Illarionova, E. V., Kuntz, J.-J., Kovalev, D. Yu., Nosyrev, A. N., Sachkova, N. V., and Tsygankov, P. A: On the mechanism of heterogeneous reaction and phase formation in Ti/Al multilayer Nanofilms, Acta Materialia, Vol**53**, pages 1225-1231, 2005.

10) Coffey, K. R., and Kumar, R: Thin Film Energetic Materials," presented at the 2nd Eglin Symposium on nano-Energetics (ESNE2), Shalimar, Florida, March 22-23, 2006.

11) Baer, M.R. and Trott, W.M: Mesoscale descriptions of shock-loaded heterogeneous porous materials, Proceedings of the 2001 APS Topical Conference on the Shock Compression of Condensed Matter, June 2001, Atlanta, GA.

12) Taylor, P.A: The Effects of Material Microstructure on the Initiation of Detonation in Solids, 22nd Annual Meeting of the Society of Engineering Science, Pennsylvania State University, Oct. 1985.

13) Tarver, C.M.; Nichols, A.L. III; Chidester, S.K: Critical Conditions for Impact- and Shock-Induced Hot Spots in Solid Explosives, Journal of Physical Chemistry, Vol**100**, No.14, 1996, pp. 5794-5799.

14) Benson, D.A., Bickes, R.W., Jr. and Blewer R.W: A Tungsten Bridge for the Low Energy Ignition of Explosive and Energetic Materials, U.S. Patent 4,976,200, Dec. 1990.

15) Baginski, T.A. and Parker, T.S: Method of Forming Radio Frequency and Electrostatic Discharge Insensitive Electro-Explosive Devices, U.S. Patent 6,272,965, 2001.

16) Lewis D.H., Janson S.W., Cohen R.B., Antonsson E.K : Digital Micropropulsion, Sensors and Actuators A-Physical, Vol **80**, No. 2, pp.143-154, 2000.

17) Barbee, T.W., Jr. and Weihs, T.P: Method for Fabricating an Ignitable Heterogeneous Stratified Metal Structure, U.S. Patent 5,547,715, 1996.

18) Danen, W.C. and Martin, J.A: Energetic Composites and Method of Providing Chemical Energy, United States Patent, 5,606,146, 1997.

19) Mikulec, F.V., Kirtland, J.D. and Sailor M.J: Explosive Nanocrystalline Porous Silicon and Its Use in Atomic Emission Spectroscopy Advanced Materials, Vol**14**, No. 1, pp. 38-41, 2002.

20) Trott, W.M. and Erickson, K.L: Ultra- High-Speed Studies of Shock Phenomena in a Miniaturized System : A Preliminary Evaluation, Sandia National Laboratories Report, SAND97-2214, Sep. 1997.

21) Benham, R.A., Bickes, R.W. Jr.; Grubelich, M.C., Wakerbarth, D.E. and Brock, J.L: LDRD Summary Report: Part I: Initiation Studies of Thin Film Explosives Used for Scrabbling Concrete - Part II: Investigation of Spray Techniques for Use in Explosive Scrabbling of Concrete, Sandia National Laboratories Report, SAND96- 470, Nov. 1996.

22) Son S.F., Berghout H.L., Bolme C.A.,Chavez D.E., Naud D. and Hiskey M.A: Burn Rate Measurements of HMX, TATB,DHT, DAAF, and BTATz, Proceedings of the Combustion Institute, Vol**28** (pt.1), pp. 919-924, 2000

23) Takacs. L : Self-Sustaining metal-sulfur reaction induced by ball milling, J. Materials synthesis and processing, 2000, **8**(3-4)

24) Bakhshai, R. Pragai, and L. Takacs: Self-Propagating reaction induced by ball milling in a mixture of Cu_2O and Al powders, Metallurgical and Materials Transactions A, 2002, Vol **33**A

25) Zeck. J, L. Takacs, and A. Bakhahai : Like SHS, Loose powder ignition a key process within mechanochemical reaction, Goucher college, Baltimore, 2001

26) Armstrong. R. and M. Koszykowski: Combustion and plasma synthesis of high-temperature material, 1990

27) Armstrong. R : Comb, Sin. Technol, 1990, **71**

28) Armstrong R : Metall. Tran, 1992, A**23**

29) Bakhshai, V. Soika, M. A Susol, and L. Takacs : J. Solid state chem., 2000, Vol**153**

30) Michaelsent, K. Barmak and T. P. Weihs : Investigating the thermodynamics and kinetics of thin film reaction by differential scanning calorimetry, J. Appl. Phys. 1997, Vol**30**

31) Blobaum. K. J, J. M. Plitzko, and T. P. Weihs : Deposition and characterization of self – propagating CuO_x /Al thermite reaction in multilayer foil geometry, J. Appl. Phys, Vol**9**, 2003

32) Mann. B, A. J. Gavens, M. E. Reiss, D. Van Heerden, G. Bao and T. P. Weihs: Modeling and characterizing the propagation velocity of exothermic reaction in mulilayer foils, J. Appl. Phys, Vol. **82(3)**, 2003

33) Fisher, S. H., and Grubelich, M. C : Theoretical energy release of thermites, intermetallics, and combustible metals, presented at the 24th International Pyrotechnics Seminar, Monterey, CA, July 1998, SAND98-1176C.

34) Wu. J. M, and Z. Li : Nanostructured composition obtained by mechanically driven reduction of CuO and Al powder mixture, J. Alloys, Vol**299**, 2000

35) Ying. D. Y, and D. L. Zhang: Solid state reaction between CuO and Cu and Al, Material Sin, 2003,Vol **361**

36) Ma Minglinang, Liu Xin kuan, Xi Sheng, and Chai Dongliang: Effect of material characteristics on the ignition of combustion reaction induced by ball milling, J. Materials, Vol**116,** 2001

I

37) Sheridan. E, and Hugus. D: Spectroscopy measurement in thin energetic film, Private communication, 2004.

38) Thaddeus. B. and Massalski : Binary alloy phase diagrams, ASM. 2000, Vol**1**

39) Turns S.R : An introduction to combustion, John Wiley &sons, New York, 1999

40) Glassman, J : Combustion theory, 2th Ed., Academic press, San Diego, CA, 1996

41) Khina, B, B., Formanek, B. and Solpan, I : Limits of applicability of the "diffusion-controlled product growth" kinetic approach to modeling SHS, Physica B, Vol**355**, pages 14-31, 2005.

42) Zanotti. C, Giuliani. P, Monagheddu. M, and Bertolino. N : Modeling of ignition phenomena in combustion synthesis, 9th ICNC-Sorrento, 2002

43) Cowan, R. S., and Winer, W. O: Frictional Heating Calculations, in *ASM Handbook, Volume 18 Friction, Lubrication, and Wear Technology*, ASM International, pp. 39–44.

44) Yovanovich, MM: Thermal Constriction Resistance Between Contacting Metallic Paraboloids: Application to Instrument Bearings, AIAA Progress in Astronautics and Aeronautics: Heat Transfer and Spacecraft Control, 24, J. W. Lucas, ed., MIT Press, pp. 337–358.

45) Yovanovich, MM: Simplified Explicit Elastoconstriction Resistance Expression for Ball/Race Contacts, AIAA Paper 78–84.

46) Bejan, A : Theory of Rolling Contact Heat Transfer, ASME J. Heat Transfer, **111**, pp. 257–263.

47) Tian, X., and Kennedy, F. E : Maximum and Average Flash Temperatures in Sliding Contacts, ASME J. Tribol. **116**, pp. 167–174.

48) Neder, Z., Varadi, K., Man, L., and Friedrich, K :Numerical and Finite Element Contact Temperature Analysis of Steel-Bronze Real Surfaces in Dry Sliding Contact, *ASME/STLE Tribology Conference*, Toronto, Canada.

49) Cameron, A., Gordon, A. N., and Symm, GT: Contact Temperatures in Rolling/Sliding Surfaces, Proc. R. Soc., London, Ser. **A268**, pp. 45–61.

50) Carslaw, H. S., and Jaeger, J. C: *Conduction of Heat in Solids*, Oxford University Press.

51) KUO, K.K.: Principles of combustion, John Wiley &sons, New York, 1986.

52) Mallard, E., and Le Chatelier, H.L: Annals of mines 4, 379-568(1883)

53) Jaeger, J. C : Moving Sources of Heat and Temperature at Sliding Contacts, Proceedings of the Royal Society, New South Wales, **76**, pp. 203

54) Rosenthal, D: The Theory of Moving Sources of Heat and Its Application to Metal Treatments, Trans. ASME, **68**, pp. 849–866.

55) Weichert, R and Schonert, K : Temperature distribution produced by a moving heat source, Mech. Appl. Math., Vol. XXXI pt .3, 1978

56) Muzychka, Y. S. and Yovanovich, MM : Thermal Resistance Models for Non-Circular Moving Heat Sources on a Half Space, Transactions of the ASME, 2001, Vol**123**, pp 624-632

57) Mandal. S, and Williamson. K: A thermo-mechanical hot channel approach for friction stir welding Journal of processing technology, 174, pp 190-194, 2006

58) Alexander. S, Tappan. A.S, Gregory T. Long, Anita M. Renlund and Stanley H. Kravitz: Micro Energetic Processing and Testing to Determine Energetic Material Properties at the Mesoscale, AIAA .2003

59) Rossi C, Do Conto, T., Esteve, D. and Larangot, B: Design, Fabrication and Modelling of MEMS-Based Microthrusters for Space Application, Smart Materials and Structures, Vol10, No. 6, Dec. 2001, pp.1156-1162.

60) Patankar S.V: Numerical Heat Transfer and Fluid Flow, Mc Graw Hill, 1980.